THESIS

NUMERICAL SIMULATION OF OUT-OF-PLANE DISTORTION FATIGUE CRACK GROWTH IN BRIDGE GIRDERS

Submitted by

Paula A. Miller

Department of Civil and Environmental Engineering

In partial fulfillment of the requirements

For the Degree of Master of Science

Colorado State University

Fort Collins, Colorado

Summer 2014

Master's Committee:

Advisor: Hussam Mahmoud

Paul Heyliger
Kelly Strong

ABSTRACT

NUMERICAL SIMULATION OF OUT-OF-PLANE DISTORTION FATIGUE CRACK GROWTH IN BRIDGE GIRDERS

Aging of the United States infrastructure systems has resulted in the degradation of many operational bridge structures throughout the country. Structural deficiencies can result from material fatigue caused by cyclical loadings leading to localized structural damage. While fatigue crack growth is viewed as a serviceability problem, unstable crack growth can compromise the integrity of the structure. Multi-girder bridges designed with transverse cross bracing systems can be prone to distortion fatigue at unstiffened web gaps. Cracking is exhibited within this fatigue prone region from the application of cyclical multi-mode loadings. Focus of fatigue analysis has largely been directed at pure Mode I loading through the development of AASHTO fatigue classifications for crack initiation and the Paris Law for crack propagation. Numerical modeling approaches through the ABAQUS Extended Finite Element Method offers a unique avenue in which this detail can be assessed. Finite element simulations were developed to first evaluate the applicability of the Paris Law crack propagation under multi-mode loading against experimental data. Following the validation, fatigue crack growth in plate girders with various web gap sizes was assessed due to mixed-mode loadings. Modeling results showed enlargement of horizontal initial crack lengths within stiffer web gap regions arrested crack development. Crack directionality was also seen to change as initial crack lengths were increased. From this research it is hypothesized that deterioration of the transverse stiffener connection can be

minimized by increasing the horizontal length of initial fatigue cracks. Enlargement of the crack plane away from regions of localized stress concentrations within the web gap may result in arrestment of the out-of-plane distortion induced cracking.

ACKNOWLEDGEMENTS

I would like to express my gratitude to my advisor; Dr. Hussam Mahmoud, for his continuous support of my research. I am indebted to the patience, enthusiasm and knowledge that he bestowed upon me. My sincere thanks also goes to the additional members of my committee: Dr. Paul Heyliger and Dr. Kelly Strong. Thank you for supporting my research and the interest that you have given to my education and the progression of this research project.

I would personally like to thank my family for their faith, prayers, and the daily support that they have given me. To my parents who inspire me daily, my sister who encourages me with such a fierce passion, and to my brother for his calm demeanor in assisting me through all aspects of this research. I am forever grateful. Finally, I offer this project to my God and savior, Jesus Christ, without whom my life would not have meaning or purpose.

TABLE OF CONTENTS

CHAPTER 1

INTRODUCTION

1.1 General Background

Completion of the Interstate Highway System ushered in an age of vitality and efficiency into the United States infrastructure system. Through the implementation of Dwight D. Eisenhower's 1938 vision of a national corridor system, both civilian and military cross country automotive transport became a reality. Currently over 600,000 operational bridges, with an average age of 42 years, exist throughout the United States (ASCE 2013). Over the years many of these bridges designed for a fifty year service life have fallen into a state of degradation. An annual report published in 2013 by the American Society of Civil Engineers, ASCE, found the condition of bridges in the United States to be at a C+ rating. From this assessment it was estimated that "one in nine of the nation's bridges are deficient" (ASCE 2013).

A predicted two hundred million trips are taken across deficient bridges within the country's largest metropolitan areas each year (ASCE 2013). Urban areas are not alone in unsatisfactory bridge qualities. In 2009, 82% of the bridges on the deficient list were found in rural areas (ASCE 2013). Substantial work has been done to address the declining state of the bridge infrastructure. Percentages of bridges considered structurally inadequate and those considered functionally obsolete dropped from previous ASCE reports. Investments within all levels of government towards bridge rehabilitation efforts, however, are currently "not keeping pace with the growing cost of aging bridges" (ASCE 2013).

One of the main factors leading to structural degradation in steel bridges is the application cyclical loadings which result in localized damage of the material. Throughout bridge service life repetitive loadings have the ability to produce fatigue cracks at critical connection details. Multi-girder steel bridge systems designed with transverse cross bracings can be especially prone to fatigue cracking. Transverse cross bracings connecting adjacent girders are intended to stabilize the bridge during construction and are typically retained once the bridge is open to traffic. Connection of these members to bridge girders is commonly achieved through the use of connection plates welded to a girder plate. Until the 1980's connection plates were cut short of the girder flanges thereby introducing inherent un-stiffened web gaps. This construction methodology was instigated as a preventative measure against primary cyclical stresses acting on the superstructure (Fisher and Keating 1989).

Over time, fatigue cracking can begin to develop within this secondary fatigue-prone detail as effects of adjacent girder differential displacements are transferred to the transverse stiffener system. Due to the un-stiffened nature of the web gap region, the differential displacements result in concentrated deformations that give rise to high localized stress levels. As loading cycles occur, the web is pulled out-of-plane resulting in tensile and bending stresses at the face of the member. This loading induces large localized deformations in the web gap region. High stresses in the web gap caused by repetitive loadings can facilitate crack growth. It is suspected that the bending stresses introduced in the web are the largest contributing factors that cause distortion fatigue cracking of this detail (Hu, Shield and Dexter 2006).

Currently there is a limited understanding of variables influencing crack growth and the rate of crack propagation for transverse connection details. Fatigue design specifications primarily consider the effects of nominal tension stresses acting on the structure. No specifications have been made specifically addressing bending or shearing action on crack development. Moreover, design of fatigue critical details focus on the fatigue life of the connection for through-thickness crack initiation. Current AASHTO LRFD Design Specifications do require the use of positive welded attachments between the transverse stiffener and the girder flange. Stiffening of the connection in this manner reduces deformations that promote crack growth. However, a predicted 85% of existing transverse stiffener systems are not connected to the flange plate (Altay, et al. 2003) giving rise to numerous reports of cracks that have developed in such details.

Studies on out-of plane distortion-induced fatigue have also largely been focused on determining the lifespan for the initiation of crack growth. Specifically, research has been conducted in an attempt to correlate nominal tension stress fatigue design codes to fatigue crack initiation of web gap details which are caused by a combination of tension and bending stresses. Knowledge of structural characteristics before cracking provides useful information that can be applied in fatigue life predictions. The current state of infrastructure and the prevalence of fatigue cracks in operation bridges demand the understanding of both crack initiation and fatigue crack growth characteristics.

This research project was directed at understanding the crack propagation characteristics within transverse stiffener systems. The framework of this study was based on the desire to link field observation and monitoring data from structural loadings with theoretical linear elastic fracture mechanics; LEFM, and numerical analyses to develop model simulations of distortion effects on web gap cracking. Through this methodology key factors in determination of crack propagation characteristics within transverse stiffener details were identified with supporting evidence from multiple aspects of analytical practices. Results of this study combined with knowledge of loadings for a specific structure can be used to enhance inspection practices and rehabilitation efforts of bridge systems containing unstiffened web gap regions.

1.2 Objectives

Research in the College of Civil and Environmental Engineering at Colorado State University was conducted to characterize fatigue crack propagation in girder web gaps. Numerical simulations were utilized to assess failure of transverse connection details and explore the effects that variation in localized geometries and loading scenarios have on this fatigue critical detail.

This project sought to achieve the following objectives;

- Investigate the use of Paris Law to simulate fatigue crack propagation rates in primarily Mode III dominate loading events;
- Study the propagation rate of distortion-induced fatigue cracks initiating in web gaps of various lengths;
- Observe crack extension patterns due to varies initial crack lengths;
- Assess the stability of crack growth under various differential displacement magnitudes;

1.3 Scope of Research

In order to achieve the aforementioned objectives, the work conducted for this research program was limited in scope in the following manner:

- Constant amplitude cyclical loading scenarios were utilized to assess fatigue resistance;
- Three test model geometries with varying web gap lengths were developed to assess cracking of transverse stiffeners;
- Horizontal initial crack lengths were varied between three magnitudes within all developed models;

- Fillet weld profiles were not included in transverse stiffener models allowing for crack propagation to occur due to solely distortion effects and not weld profiles;
- Residual stress concentrations of the detail due to welding effects were ignored as they are thought to not affect crack growth due to their orientation with respect to crack propagation direction;
- Effects due to corrosion and other environmental variables influencing fatigue resistance were not considered in the research.

CHAPTER 2

LITERATURE REVIEW

2.1 Introduction

Development of the research project involved the understanding of both the physical effects of fatigue cracking at web gap regions, and mathematical modeling techniques used to predict crack propagation. Insight into the effects of fatigue loading on the connection detail was gathered from previously conducted physical testing and field observations. Corroboration of numerical simulations used throughout the research was linked to physical testing results to ensure modeling techniques captured the physical characteristic of the failure. Justification for modeling procedures and applied analytical solutions were gathered from previously published works in the fields of fatigue and fracture mechanics.

A literature review focused on the fatigue of structural steel, current design specifications, and rehabilitation methods was conducted for the purpose of this research. Results of the review are provided in the following sections.

2.2 Fatigue Failure Theory

2.2.1 Modes of Failure

Primary causes of fatigue crack growth are attributed to continuous loading cycles, the stress range induced in the material from applied loads, and the directionality of those loads. The latter is of primary importance to the determination of the mode of loading in which a material is subject to. Experimental and field observation of material failure has led to the understanding that three principal loading modes can affect the development and directionality of cracking.

Material subjected to nominally applied stresses acting perpendicular to the orientation of the crack plane is indicative of a pure Mode I failure. Cracking patterns developed from Mode I loadings result an opening action. Delamination growth of the material characteristically progresses perpendicular to the applied stress. Reorientation of the stresses to be perpendicular to the crack front and yet parallel to the plane of the crack results in a Mode II failure. Distinguishing traits of this failure mode are noted by a shearing action as the crack faces slide against one another. Crack propagation due to out-of-plane movement between the two crack faces is indicative of the final type of loading mode: Mode III. This loading mode is classified as a tearing shear of the material. Characteristic crack propagation is identified by an out-of-plane shearing of the two crack planes. Development of Mode III cracking patterns is induced by stresses applied parallel to both the crack plane and crack face. Figure 2-1 below shows the three distinct modes of loading.

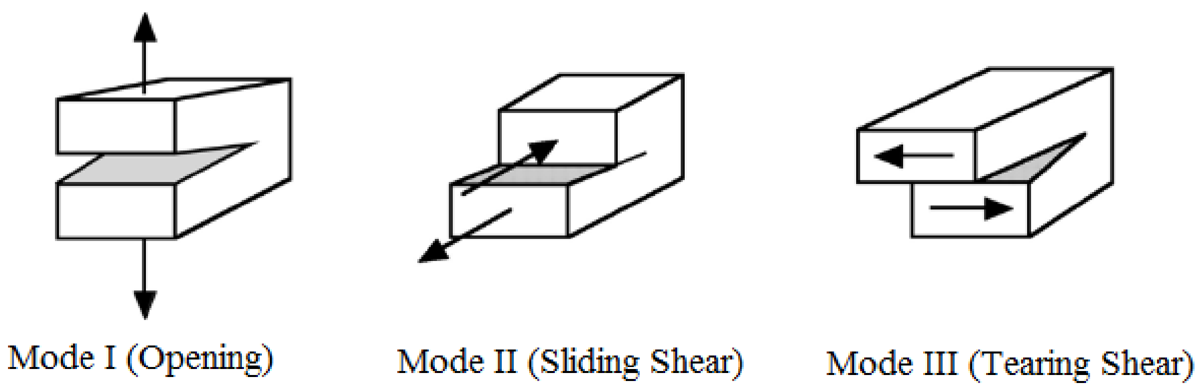

Figure 2-1 Pure Modes of Loading (Reeder 1992)

Crack propagation can be caused by a singular loading mode, or a combination of multiple mode types. Distinction of modes acting on a specimen is largely classified by loading directionality. The cyclic loading of web gap regions in bridge superstructures can be correlated to a mixed mode failure due to Modes I and III; with Mode III being the predominate mode of loading. Crack development in this multi-mode failure results from a combination of shear stresses acting parallel to the plane of the crack and normal tensile stresses perpendicular to the crack face. This is characteristic to stresses found within the web face of the diaphragm girder connection. Nominal stresses due to girder deflection develop in the web gap region and are correlated to Mode I loading effects. Bending of the web gap due to differential displacements indicate Mode III loading acting in the web girder. While Mode I loading effects are present within the web gap, it has been observed that nominal global effects are significantly smaller than out-of-plane bending. Therefore, Mode III is the primary loading mode facilitating crack propagation of transverse stiffeners. Fatigue cracking due to out-of-plane bending stresses applied to the web gap therefore governs the failure of connections (Connor and Fisher 2006). Figure 2-2 shows the distortion induced in the web gap due to the differential displacement between adjacent girders.

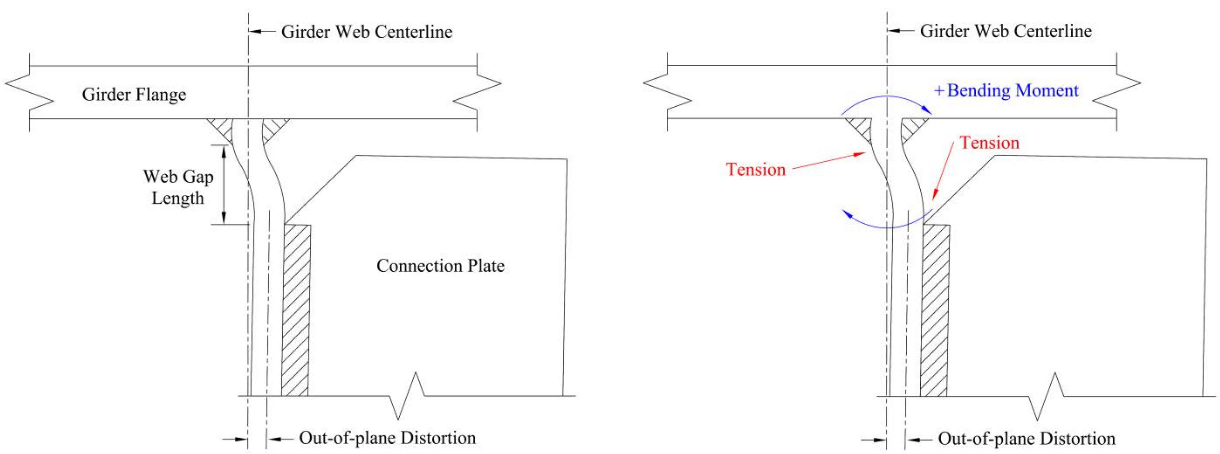

Figure 2-2 Distortion of the Girder Diaphragm Connection (Fu, et al. n.d.)

2.2.2 Fatigue Crack Life

It is important to note that not all material cracking results in structural instability. Stable crack growth can aid in alleviating stress concentrations in the material, and may cease to propagate once the magnitude of the controlling loading mode is attenuated. In cases such as this it may be more beneficial to monitor the crack while refraining from rehabilitation. Efforts meant to arrest crack propagation may do more harm than good. One important aspect in determining appropriate measures involves assessing the current character of the crack and where it is in the stages of fatigue life. Two distinct phases of crack life; initiation and propagation, are of primary interest when monitoring material fatigue. Development of cracking through these two stages leads to an understanding of the current fatigue resistance of material and if any retrofitting is advisable.

Crack Initiation

Developments of material fissure occur due to prolonged exposure to repetitive loadings. One location for crack initiation can be embedded within the thickness of the fatigued material. As loading cycles occur, dislocation planes are amassed which begin to form persistent slip band structures, PSB's (Lukáš and Kunz 2004). Along these slip planes material degradation begins through a process of extrusion and intrusion. While this process is largely invisible to observation without cross sectional fractorgraphic analysis, PSB formation denotes the initiation of fatigue cracking.

The applied stress range is the primary variable used to assess fatigue crack development rates. As cyclical loads are applied a resulting variation in stresses within the material is induced. Intuitively, higher stress ranges acting on the material result in fewer necessary loading cycles to propagate PSB structures into a crack plane. Maturity of PSB structures into micro-scale fatigue abrasions signifies the transition from crack initiation to propagation (Lukáš and Kunz 2004).

Another variable linked with the stress range application that also contributes to initiation of fatigue cracking involves the geometry of the material experiencing the fatigue loading. The presence of geometric discontinuities such as welds or grooves can result in the development of high stress concentrations. These high stress fields culminate in producing areas that are more susceptible to fatigue and leads to an accelerated time table for crack initiation.

Design of bridge structures against fatigue crack initiation to safeguard against these high stress regions was first introduced into design specifications in 1969 with the 10th edition of AASHTO Standard Specifications for Highway Bridges. Publication of the 12th edition of the AASHTO specification in 1977 identified six fatigue classes developed to characterize the fatigue life of common connection details (Bowman, et al. 2012). Correlation was made between the applied stress ranges acting on bridge components due to live load application with the number of loading cycles needed to initiate a through-thickness crack.

One manifestation of this relationship is expressed by fatigue life curves within AASHTO code specifications. These curves compare applied stress ranges to the number of loading cycles to initiate through-thickness cracks and are known as S-N curves. For each classification there is a correlating design curve expressing the fatigue life of the detail at a specified stress range. Important insight into the available service life of a connection until crack initiation can be gathered from these S-N curves. Development of these fatigue curves were specific to Mode I failure effects. Consequently, development of these design curves fails to account for Mode II, Mode III, or multi-mode effects.

Use of S-N curves has remained a primary tool to develop predicted fatigue lives of critical connections. Through the years additional classifications have been added to the original fatigue categories for a total of eight fatigue classes. Classes A through E’ shown in Figure 2-3 are primary classes used for fatigue design controls. Category F, not pictured in the figure below, is associated with fillet and plug welds with low stress ranges that rarely control design (Chen and Duan (Eds.) 2014).

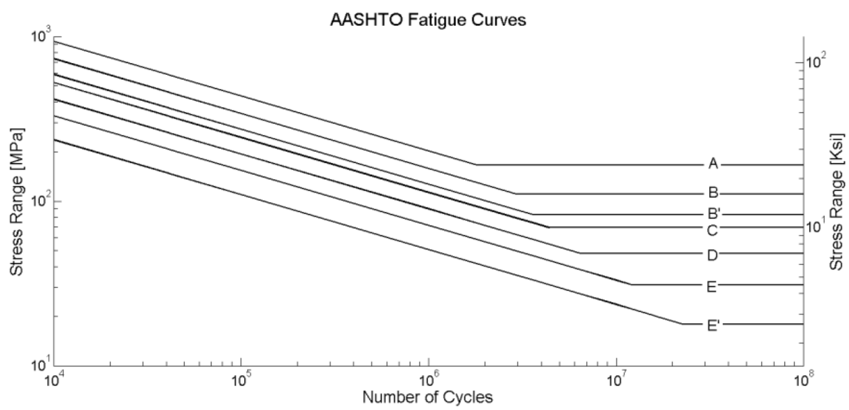

Constant Amplitude Fatigue Limit	
Class	Stress Range [Ksi]
A	24
B	16
B’	12
C	10
D	7
E	4.5
E’	2.6

Figure 2-3: AASHTO S-N Fatigue Curves

Current AASHTO S-N fatigue curves include a stress range limit below which crack initiation is understood to not occur. From experimental testing is was observed that the probability of crack initiation occurring due to low applied stress ranges for each fatigue classification was significantly reduced. In fact, it was determined that when the stress range is low enough fatigue life is effectively infinite. While an infinite fatigue life is not physically possible, low cyclical stresses acting on a connection could result in no observable crack initiation throughout the service life of the structure. Due to this observation, constant amplitude fatigue limits (CAFL), shown in Figure 2-3, for all fatigue classifications were specified to denote stress range below which fatigue life is stated to be infinite.

Fatigue curves provide an idealized estimate for crack initiation. Sensitivity of crack growth to geometric anomalies however may lead to earlier detection of crack initiation. The time required for crack initiation to occur may also decrease due to any inherent flaw in a material or connection. Welding of materials to create connection details can often result in flaws that act as initial crack locations. This can be especially common in connections such as transverse stiffeners where welding of the stiffener plate to the girder is common. Initial through thickness or surface defects can expedite crack growth, and may cause fatigue cracking at stress levels believed to be safe from initiating fatigue failure.

Crack Propagation

Propagation of a fatigue crack defines the growth of cracking after initiation yet before the eventual failure of the material through fracture. Once a crack is formed, variables developed from the stress range application are important when assessing crack stability. The magnitude of the stress range; $\Delta\sigma$, combined with the current length of the crack; a, results in the alternating stress intensity factor; ΔK, of the material. The general form of the equation used to determine the ΔK values is shown below.

$$\Delta K = Y(\Delta\sigma)\sqrt{\pi a} \tag{1}$$

Calculation of ΔK is subject to geometric considerations of the material in question. Correction factors applied to the general equation are combined within the variable Y to account for differing geometric effects.

When compared to theoretical values, computed ΔK values for a given stress range and crack length help to illustrate the stability of the crack and what stage of crack propagation the material is currently experiencing. Experimental ΔK values that denote stable crack growth exist of all of the three loading mode types. Therefore, it is important to assess the directionality of the controlling applied stress in relation to the crack plane. In doing so, it is possible to determine which mode of loading is controlling and which theoretical values to use for analysis. Three different zones of failure states, shown in Figure 2-4, exist for fatigue crack propagation.

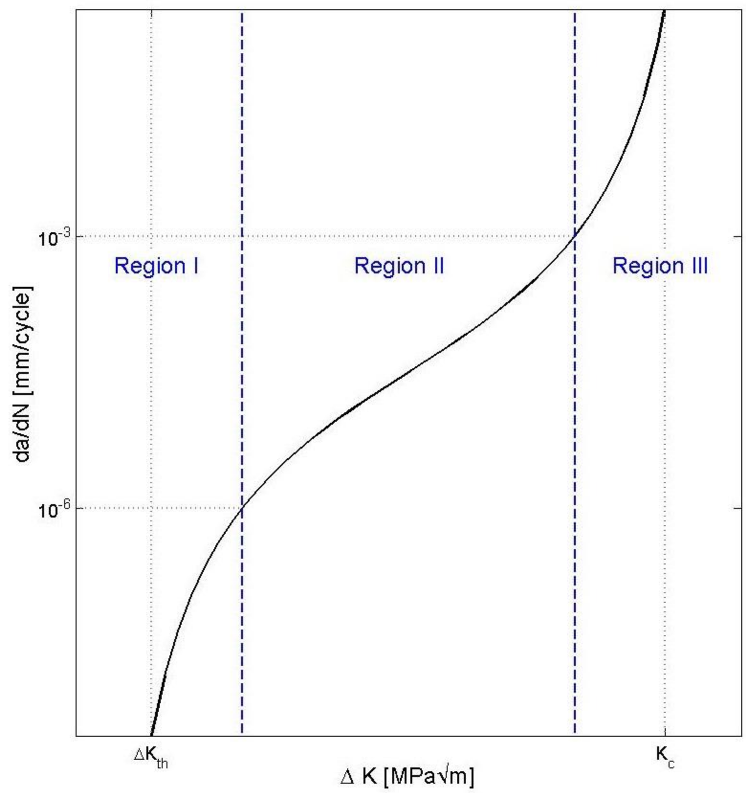

Figure 2-4 Crack Propagation Regions (Vethe 2012)

Region I defines unsteady crack growth of micro-scale fatigue cracks; short cracks. This zone of crack propagation occurs directly after crack initiation is said to occur. The growth of micro-scale cracks are caused when the ΔK of the material is near the threshold value; ΔK_{th}. On a log-log scale, the relation the crack growth rate; da/dN, versus ΔK shows a high rate of crack extension for this stage of growth.

Experimental testing is used to determine the threshold values of a specific material. Studies of the threshold intensity values for steel have noted theoretical ΔK_{Ith} values to lie between 3.626 MPa√m (3.3 ksi√in) and 5.824 MPa√m (5.3 ksi√in) (Klingerman and Fisher 1973). Research in the area of ΔK values for mild steel has noted that Mode II values are approximately 1.15 times greater than ΔK_{th} values for Mode I (Hellier, Zarrabi and Merati 2011).

Limited investigation into Mode III ΔK_{th} values has been conducted. At the time of literature review for this study no value could be determined for Mode III ΔK_{th}. Due to the nature of the loading mode, it was hypothesized that Mode III ΔK_{th} values would be greater than Mode I. This proposition steams from the understanding that non-Mode I loaded geometries often are subject to crack ratcheting effects that can result in crack closures thereby delaying crack development. Mode III ΔK_{th} would therefore need to be greater in magnitude to result in crack propagation.

When threshold ΔK values are exceeded due to a combination of the applied stress range and crack length, the second classification of crack propagation is reached. Region II of crack development is most notably defined by a state of steady crack growth and denotes the primary region studied when modeling crack propagation; see Figure 2-4. Focused attention in this region of crack growth is generally accepted as it customarily models the longest segment of crack propagation. Various analytical models have been developed to represent crack growth in this region. The most widely used of which is the Paris Law (1961).

Region III defines unsteady crack growth when the maximum stress intensity within a loading cycle nears the critical fracture stress intensity of the material; K_C. Ultimate failure of the material occurs at the end of this region when the maximum stress intensity factor is greater than the critical value of the material in question. K_C of a material is determined through experimental testing and is subject to change based on acting loading modes. Impact strength testing with the Izod or Charpy V Notch method is the primary manner in which Mode I fracture toughness values are determined for a given material (Yue 2009). Room temperature measurements of the K_{IC} have determined a theoretical value of 50 MPa√m (45.80 ksi√in) (Dr. Abadi n.d.). Variation in critical values for loading Modes II and III have been studied providing a resulting ratio of values. Experimentation of steel failures identified a 1:0.8:0.7 relationship between the K_C values for Mode I, Mode II, and Mode III (Jie-Oing 1989).

2.2.3 The Paris Model

In 1961 Paul Paris in conjuncture with his colleague Fazil Erdogan introduced the theory that the rate of crack growth per number of loading cycles could be correlated to ΔK_I values (Paris, Gomez and Anderson 1961). Upon the examination of numerous material fatigue cracks due to Mode I loading it was noted that, on a log-log scale, a straight line equation could be used to predict the growth rate of a crack in the second region of crack development. This relationship allows for the quantitative prediction of residual life of loaded materials by correlating the growth rate to the alternating stress intensity factor with the use of equation constants C and m in the following manner.

$$\frac{da}{dN} = C(\Delta K)^m \qquad (2)$$

The constants of this equation are representative of both material characteristics and environmental factors affecting crack growth. The slope of the straight line fit represents the constant variable m while the intercept of the linear fit is indicative of the C constant in the Paris Law equation. Figure 2-5 depicts the application of the Paris Law propagation rate equation to the second region of crack growth.

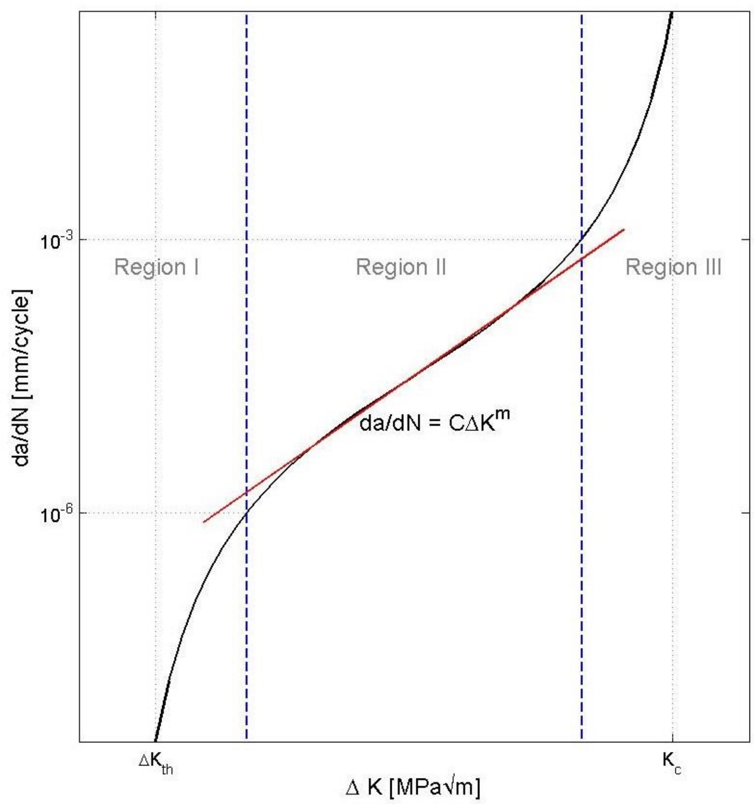

Figure 2-5 Paris Law Fatigue Equation Relationship (Roylance 2001)

Calibration of this model for test material is performed via comparison to experimental data. For structural steel material the slope of Paris' model and subsequently the value for the equation constant; m, has been noted to be approximately equal to 3.0 for Mode I loaded details (Gilmour and et.al. 2004). The equation constant; C, actively determines the nature of the predicted crack growth rate. Experimental research has yielded that this constant experiences significant fluctuation within testing results. Researches in the field of fatigue failure largely attribute the variation in C values to scatter within fatigue testing (Gilmour and et.al. 2004).

The Paris Law has been widely accepted as a viable and versatile crack growth propagation model for a multitude of materials. However, the straight line fit of the model restricts the viability of application to region II of the crack growth life. Application of the model to crack growth where the alternating stress intensity factor approaches the threshold value leads to overestimation of the crack growth rate. As the maximum K value in a loading cycle nears K_C, the predicted growth rate will be conservative. Therefore the implementation of Paris' Law is restrained to growth rates between 10E-3 mm/cycle and 10E-6 mm/cycle to avoid nonlinearity in the crack growth behavior (Vethe 2012).

2.3 Cracking of Bridge Girders due to Distortion-Induced Fatigue

2.3.1 Background Information

Predominant crack growth is found within web gap regions of transverse connection details due to localized bending stresses resulting from out-of-plane deformations (Fisher 1990). Within multi-girder bridge structures, the interaction of transverse stiffeners to bridge girder members is the primary interface facilitating fatigue cracking. Transverse cross bracings connecting adjacent girders are utilized during construction processes to stabilize the bridge, and are typically retained after the bridge is opened to traffic. Often these members are maintained in an effort to transversely distribute vertical traffic loads and laterally applied wind loads. (Castiglioni, Fisher and Yen 1988)

Conventional union of these members to bridge girders is commonly achieved through the use of connection plates welded to a girder plate. Until the 1983, positive connection of the stiffener plate to the girder flanges was avoided. This method was developed from efforts to prevent "fatigue-sensitive weldments" that caused numerous fractures of European bridges in the 1930's (Fisher and Keating 1989). While improvements to both welding processes and materials have removed the primary causes of these fractures seen overseas, a large number of operational bridges in the United States contain these fatigue prone web gap details.

Cyclical loading of multi-girder bridge superstructures have the potential to induce differential displacements of adjacent girders. High stress levels develop in the web gap region from out-of-plane distortion resulting from the girder displacement. Overtime the relative movement of neighboring girders coupled with the unstiffened web gap region can produce fatigue cracking in the girder web. Cracking of these details have been seen to occur over a short duration of time. Observations have been made of transverse stiffener details developing fatigue cracking within the first decade of service (Fisher and Keating 1989). In some cases cracking was noticed at the ends of transverse stiffeners during the construction of the bridge superstructure (J. W. Fisher 1978).

2.3.2 Studies of Distortion-Induced Fatigue Crack Propagation

Studies on the initiation of fatigue cracking have resulted in the determination that fatigue resistance of the web gap region can be classified using the AASHTO S-N fatigue curves. Although distortion of transverse stiffener connections is characteristic of a mixed Mode I and Mode III loading, the fatigue resistance of the web gap is defined in the 1977 AASHTO specification as a category C detail. This designation was determined based on small scale testing of flange to web boundary simulations. Results of studies by P. Goerg (1963) and Muller & Yen (1968) show that fatigue cracking at the web gap was initiated at loading cycles above those determined for category C details at specified stress ranges (J. W. Fisher 1978). A cyclical testing program conducted in 1979 further examined damage caused by distortion effects. Testing was specifically conducted on web gap regions without a positive attachment to the girder flange. Crack initiation data collected from this test reiterated the fatigue life of the connection to be above that for category C (Fisher, et al. 1979). Fatigue life classification of transverse stiffeners has therefore created a lower bound estimation of fatigue resistance (J. W. Fisher 1978).

Propagation of fatigue cracks of transverse stiffener details are largely subject to the geometry of the surrounding detail in addition to the displacement induced stresses. Due to the complexity of the structure it can be difficult to assess the effects that these two parameters will have on a connection detail (J. W. Fisher 1978). Field monitoring of transverse stiffener connections isolated four general crack patterns that are exhibited in fatigue of web gap regions.

One common location for crack initiation is seen to occur within the interface of the stiffener and girder web at the fillet weld material (J. W. Fisher 1978). Progression of fatigue crack growth within this classification tends to follow the boundary of the fillet weld. Once the crack has progressed horizontally along the weld line extension can occur into the web material. A cross sectional examination of cracking within this connection also noted that cracks progress into the thickness of the web as it grows horizontally. Directionality of the crack extension can curve vertically once the crack plane extends into the web thickness (J. W. Fisher 1978). Planar and cross-sectional views of the crack profile described above have been illustrated in Figure 2-6.

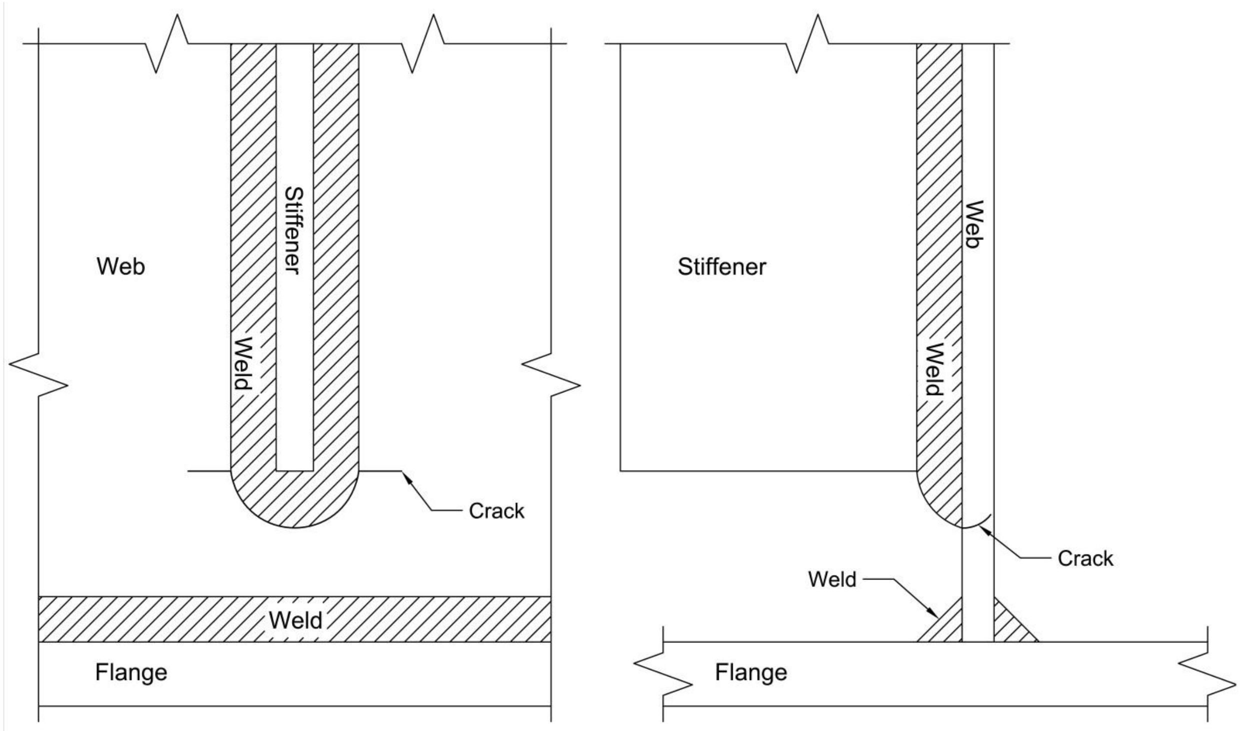

Figure 2-6: Variations of Fatigue Crack Growth (J. W. Fisher 1978)

Rather than initiating at the weld to girder interface, cracking can also be observed to occur within the weld material itself. This failure type may be due to unsatisfactory welding of the connection that resulted in an embedded flaw that served as the location for crack initiation. Patterns of crack growth in this case show full extension across the weld material, and into the girder web (J. W. Fisher 1978). Curvature of cracking is common in this type of failure once the crack has extended into the girder. Samples taken from bridge superstructures with this failure type give evidence of cyclical loadings being the primary factor causing fatigue. Apparent tearing of the girder material is also commonly observed in plugs taken from bridge superstructures (J. W. Fisher 1978).

The presence of welding within this connection detail provides yet another avenue for crack propagation. Rather than progressing horizontally with a slight vertical curvature, cracking can also occur along the vertical weld interface of the stiffener and the web. Breaks within the fusion of the weld connecting the stiffener and girder members are a primary cause for this failure (J. W. Fisher 1978). As cracking progresses the cyclical loading on the connection can “peel the weld away from the web surface” (J. W. Fisher 1978).

High stresses caused from differential displacements can also lead to crack formation within the girder at the web gap region. Initiation of this type is not noted to be affected by connection fillet welds (J. W. Fisher 1978). It is also not seen to be a propagation of cracking from within the weld material. Failure initiates as a surface crack, and as the length of the crack increases the crack plane also propagates into the web material. This crack propagation was the focus of study for this research. Theoretically this cracking classification can be modeled after as a thumbnail growth. As the length of cracking extends both along the surface and into the thickness of the material, the crack plane resembles a half circle or “thumbnail”. This results in the horizontal extension of the crack; 2c, being approximately twice as long as the growth through the thickness of the material; a, as shown in Figure 2-7.

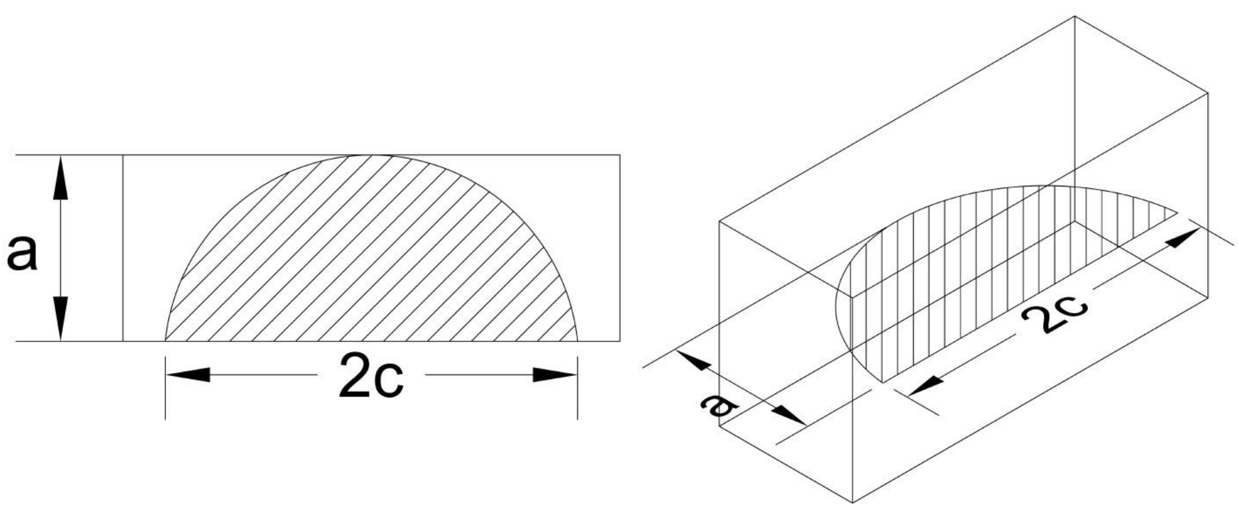

Figure 2-7: Embedded Thumbnail Crack Profile

Assessment of bridge superstructures has also shown that the crack profile can extend through the web gap region and into the weld interface of the web and flange sections. Branching of crack planes has also been known to occur. This can result in a multitude of the crack profiles discussed above being present in any given web gap. Variation of crack profiles is one reason in which assessing out-of-plane distortion can become so complex, and lead to multiple views on appropriate measures to take in retrofitting connection details. Several of the crack profiles mentioned above can be seen in Figure 2-8.

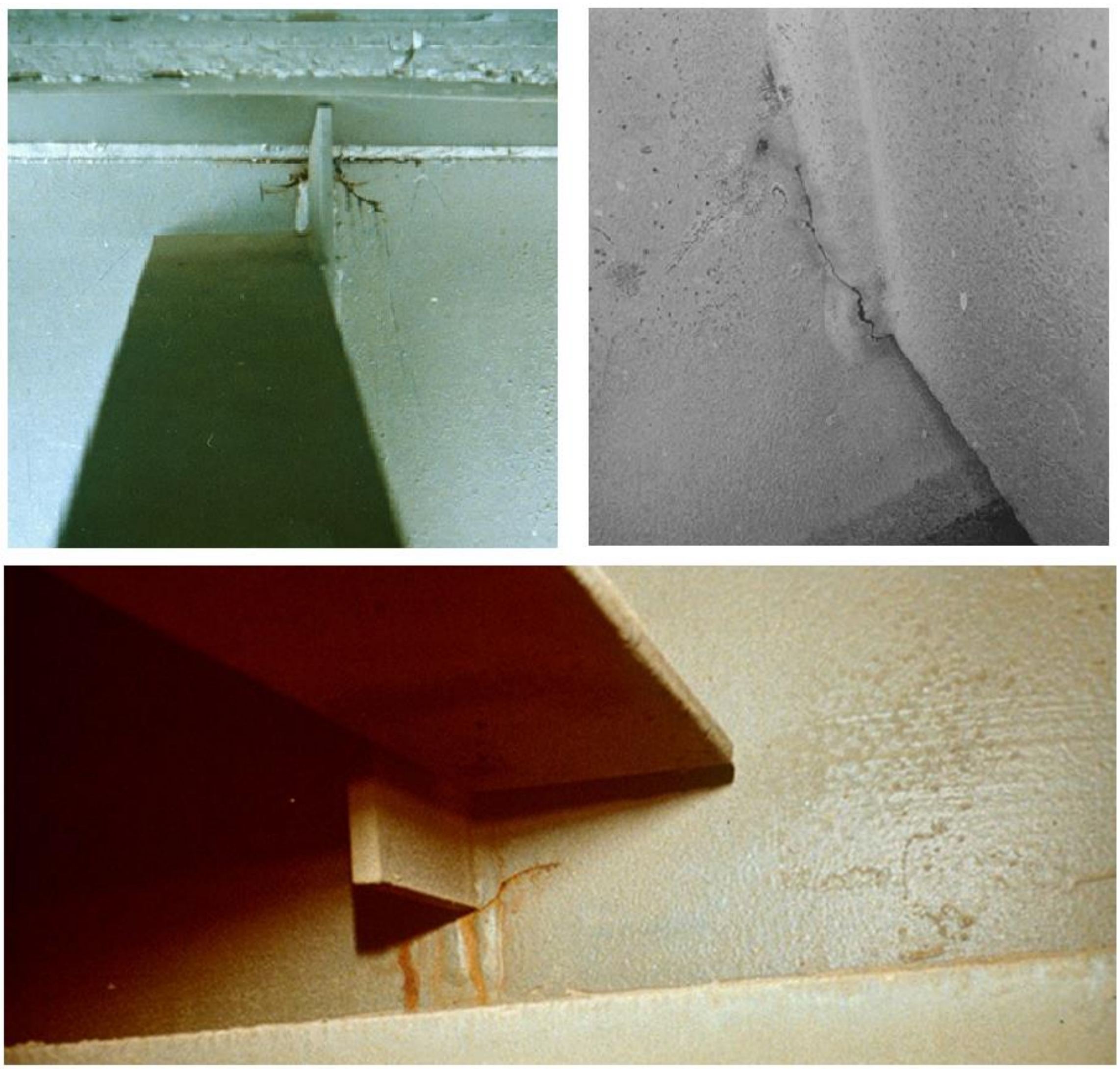

Figure 2-8: Fatigue Crack Profiles (D. H. Mahmoud 2013)

Analysis of fatigue cracking has determined three primary conditions that are present with distortion-induced fatigue prone details. The combined presence of an unstiffened gap, out-of-plane deformation, and constraint of the boundary create an ideal location for crack development (Fisher and Keating 1989). Fatigue cracking when these conditions are present is not confined to any one bridge configuration. It has been noted that multi-girder, box-girder, and tied-arch structures are all susceptible to distortion-induced cracking (Fisher and Keating 1989).

Studies of stress levels acting on the connection have also been found to alter the cracking response of the material. Field monitoring of bridge superstructures observed that typical relative out-of-plane displacements of the connection plate versus the girder flange measure 0.013 to 0.025mm. This displacement induces bending stresses with magnitudes between 10 and 97 MPa (1.45 and 14.07 ksi) (Fisher and Keating 1989). Laboratory studies evaluating relative out-of-plane distortions in addition to stress effects in the web gap allowed for closer analysis of transverse stiffener detail fatigue. Crack initiation of web gaps were noted to develop after 1.3 million cycles when maximum stress ranges of 180 MPa (26.10 ksi) were present in the web gap region. Reducing the applied load to result in 134 MPa (19.43 ksi) bending stresses in the web gap increased the detail fatigue life to 5.0 million cycles before crack initiation (Fisher and Keating 1989).

Numerical investigation of web gap effects on out-of-plane distortion fatigue showed that lengths of this region also affected fatigue resilience. By varying the magnitude of the web gap length to girder thickness ratio; g/t_w, it became possible to develop the local behavior of the web gap in addition to the localized stresses induced by out-of-plane displacement effects (Castiglioni, Fisher and Yen 1988). Results of the study showed that the presence of a web gap, no matter how long, resulted in significant concentrated deformations (Castiglioni, Fisher and Yen 1988).

Changes in the web gap length alone were noted to do little to alter the magnitude of the out-of-plane displacements. However, when the girder thickness was increased for a set web gap length, the displacements were seen to noticeably decrease. Additionally it was noticed that distortions resulting from transverse effects were focused in a region approximately 4 to 5 times the web gap length (Castiglioni, Fisher and Yen 1988).

Primary results of Castiglioni's work illustrates that concentrated deformations develop within bridge girders with the presence of an unstiffened web gap. While the web gap length did little to alter the magnitude of the resulting deformations, cutting back the stiffener member to elongate the web gap would decrease the high stress concentration in this region. It was hypothesized that this reduction in stress may result in the arrest of fatigue crack growth. Alterations to the transverse connection detail were also noted to minimally affect global system performance. A finite element modeling of bridge superstructures showed that localized variation in bridge geometry, such as the web gap length, resulted in only small global variations. It was reported that global results "were not influenced by varying a local parameter" such as the girder web thickness (Castiglioni, Fisher and Yen 1988).

2.4 Current Design Requirements & Coding Practices

2.4.1 Design Guidelines

Specifications for fatigue design of bridge structures have only been instigated in code practice in the past 50 years. The lack of fatigue life considerations prior to this time is one primary contributing factor to the fatigue deficiency of currently operational bridges. Current specifications design for a 75 year fatigue design life by considering effects due to loading frequency and the fatigue resistance of members within the bridge geometry (Grubb and Schmidt 2004).

Differentiation within design guidelines exist for LRDF and AASHTO specifications, however, the general outline for fatigue design follows the same trend. Fatigue classifications are assigned to each connection and detail to be used within the structural layout. AASHTO specifications rely upon eight classes of fatigue resistance A-F. These categories were developed based on the applied stress range, number of loading cycles, and detail category (Bowman, et al. 2012). Classes with a higher letter, i.e. F, correspond to details that are more prone to crack initiation. Current methods for fatigue strength evaluation of web gap details are based on AASHTO category C detail classification.

Fatigue design also considers fatigue loading that will act on the structure. It has been determined that live loads due to truck traffic moving over the bridge surface is the primary cause for fatigue of bridge components. LRDF bridge design codes apply a single design truck upon the bridge to assess fatigue loading with a load factor of 0.75. This design truck load has been developed to represent a variety of truck loads anticipated to act on the bridge layout. In contrast AASHTO guidelines apply an AASHTO HS15 loading to assess fatigue of the bridge. From the applied load a live-load stress range is then reported and used in further steps of the design process (Grubb and Schmidt 2004).

Evaluation of the fatigue stress range is compared to the average daily truck traffic (ADTT) that is expected to cross over the bridge deck. This value correlates to the total number of fatigue loading cycles anticipated to act on the bridge in one day. Multiplication of this value by the total fatigue design life; 75 years, determines the total anticipated fatigue loading cycles to act on the bridge throughout the design service life. The fatigue resistance of a connection is then compared against the applied fatigue stress range to determine if fatigue life of the connection is adequate for this number of loading cycles. One manner in which this assessment is made is based off of the AASHTO S-N curves previously mentioned. If the fatigue resistance of the most critical connection is adequate under this stress range and loading cycles, all other connection classes are said to be sufficient as well.

Current AASHTO codes indicate that the manifestation of distortion-induced fatigue is "a stiffness problem…versus a loading problem" (Bowman, et al. 2012). In an effort to eliminate the number of web gap fatigue failures, AASHTO and LRFD coding practices require positive attachment of the connection plate and both girder flanges (Grubb and Schmidt 2004). A coping length of the larger of two inches or four times the web thickness in the connection plate is also required as a preventative measure to fatigue cracking (Hu, Shield and Dexter 2006). While these anticipatory methods are helping to stem occurrences of fatigue cracking in current bridge design, a predicted 85% of operational bridges are currently without these protective measures (Altay, et al. 2003).

2.4.2 Inspection Guidelines

Continual monitoring and inspection of bridge superstructures is vital to maintain consistent observation of any critical bridge connection or detail. Bridge components determined to be fracture critical members are given special attention; however, the entire superstructure must be inspected to ensure integrity (Ryan, et al. 2012). Federal Highway Administration requirements specify an inspection frequency not exceeding twenty-four months (Federal Register Rules and

Regulations 2004). This allows for constant observation of those members and connections which may be considered fracture or fatigue critical.

Both visual and physical inspections of bridge members determine the current state of the infrastructure. Detection of cracking within a member through optical examination is possible, and is the primary method in which cracking is first detected (Ryan, et al. 2012). Further analysis of crack status can be obtained through physical, non-destructive testing. Physical inspection of the components can include removing debris from the area, and assessing the depth of crack penetration into the material. One test used to assess crack characteristics accentuates the crack profile through application of a dye (Ryan, et al. 2012).

Adequate documentation of current field conditions is another vital tool in assessing crack progression. Thorough recordkeeping of all inspections and retrofits made upon a bridge member allow for analysis of the rate of crack growth. Countermeasures performed to combat the crack growth must be recorded. Assessment after a retrofit is applied to a bridge must include observations of the retrofit and note any further crack growth in the area. Documentation upon inspection of a defect should include the following information (Ryan, et al. 2012);

- Method of inspection;
- Date deficiency was first detected;
- Type of deficiency;
- Detailed schematics of location and geometry of deficiency;
- Deformations occurring in the surrounding material due to load application;
- Updated information on maturity of a deficiency upon each subsequent inspection;
- Weather conditions at the site of inspection;

2.4.3 Rehabilitation of Transverse Stiffeners

In the event that fatigue cracking does occur at the transverse stiffener interface, several retrofitting options have been developed to combat additional crack extension. Differing schools of thought exist for the best way to attenuate fatigue effects. One approach is to decrease the distortions occurring in the web gap by stiffening the connection detail. Another theory is that reduction in stresses acting on the region will also successfully suspend crack growth.

Stiffening of the web gap region is used to minimize out-of-plane distortions. Positive contacts between the girder flange and transverse stiffener plate add stiffness to the detail that helps to mitigate deformations. Sections used to stiffen the connection are not limited by geometry. Documented cases of stiffening retrofits have utilized single or double angles, and WT shapes.

Studies of bolting angle members to the stiffener and flange plates showed that connector stiffness rather than material strength drove the success of the retrofit (Connor and Fisher 2006). Additional work noted that application of WT and paired angles aided in slowing crack growth. Retrofitting transverse connections in this fashion does result in stress concentrations forming within the web gap. While deformation magnitudes are lessened, cracking was seen to initiate quickly in the web material. However, due to the smaller distortion effects, crack growth slowed as it propagated away from the web gap due to a softening of the connection (Bowman, et al. 2012). Figure 2-9 shows one methodology used to stiffen transverse connection details that are not welded to the girder flange.

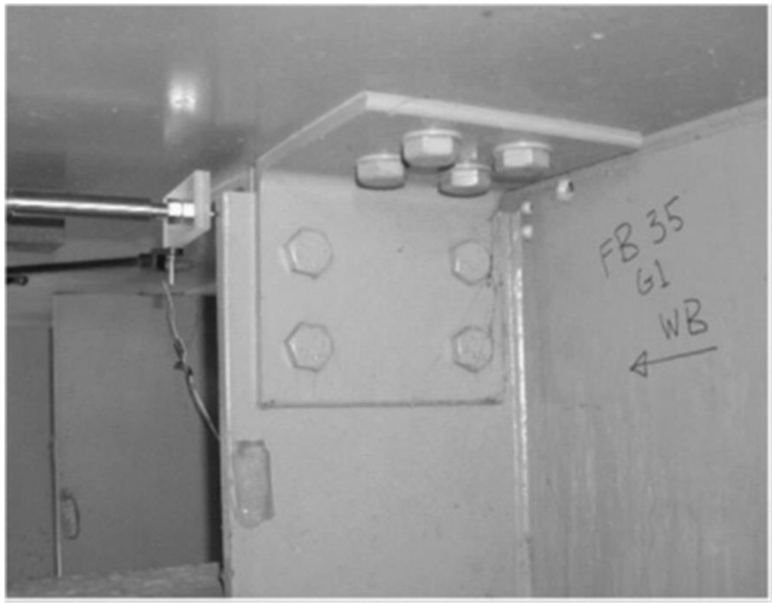

Figure 2-9: Stiffening Rehabilitation of Transverse Stiffener (Connor and Fisher 2006)

Intentional softening is another way in which the transverse stiffener connection can be retrofitted. As previously mentioned, crack growth was seen to slow once the crack extension softened the connection by a certain amount. Lengthening of the web gap region by flame cutting the stiffener plate is one way in which web gap connections are softened. This method is often used in conjunction with hole drilling retrofits before cracks have propagated a significant amount. With this modification there is a possibility that increased web flexibility might adversely affect the integrity of the connection and result in increased distortion (Fisher and Keating 1989). If this is the case, crack propagation may not be arrest and may in fact increase in growth rate. Figure 2-10 shows application of the softening retrofit technique on a transverse stiffener connection, and a fatigue crack that has extended after the retrofit was applied.

Figure 2-10: Softening Rehabilitation of Transverse Stiffener (D. H. Mahmoud 2013)

Another possible approach to arrest crack propagation is through the application of holes drilled within the cracked material. By capturing the crack tip within the drilled hole, stress concentrations at the crack tip are released, and cracking is reduced The hole drilling method is known to be effective for mitigating cracking under Mode I loading, but not as effective for other loading modes. Experimental studies showed that drilled holes arrested cracks when the following relationship was maintained;

$$\frac{\Delta K}{\rho} < 4\sqrt{\sigma_y} \quad (3)$$

Hole drilling retrofits require knowledge of the alternating stress intensity factor; ΔK, at a given in-plane bending stress range; S_r, and the yield strength; σ_y, of the material in units of ksi. The hole radius; ρ, needed to arrest the crack is determined so that the relationship shown above is maintained (J. W. Fisher 1990).

Hole drilling techniques can be applied in addition to stiffening or softening of the web gap, or can be applied independent of these two retrofitting methods. Evidence of drilling can be seen in

Figure 2-9 in conjuncture with stiffening countermeasures. Use of drilling as the sole countermeasure is only advisable when deformations are low, and the crack has propagated into a low stress region of the material. Premature drilling of the crack may not stop crack extension from occurring. Care must also be taken to ensure that the entire crack tip is captured within the drilled hole (Fisher and Keating 1989). Locating the entire crack tip may be difficult to judge as crack plane directionality can change within the material thickness without any visual evidence. Hole retrofitting is not considered a permanent solution for crack arrestment. Re-initiation of cracking past location of holes that satisfy equation 3 have been noted in field observations (Fraser, Grondin and Kulak 2000). Repetitive drilling of holes has been applied in bridge superstructures, see Figure 2-11, but analysis must be conducted to ensure that structural stability has not been compromised due to the retrofit.

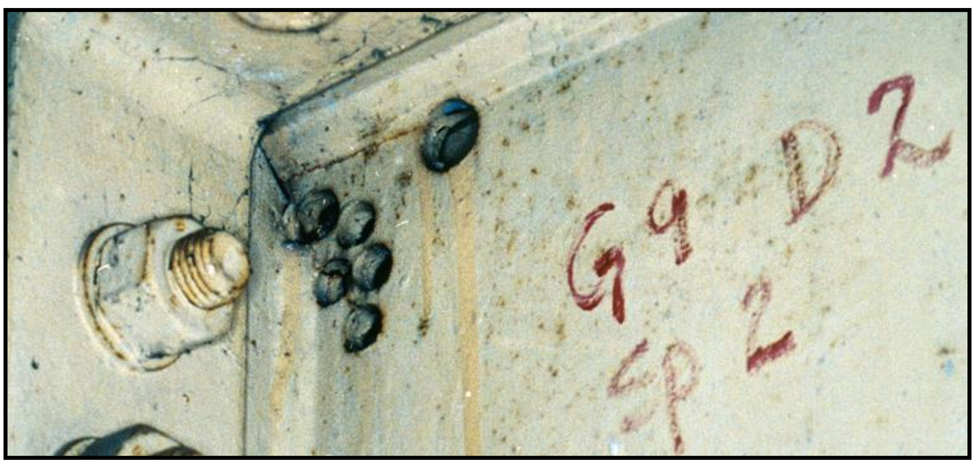

Figure 2-11: Repetitive Application of Hole Drilling Retrofit (D. H. Mahmoud 2013)

2.5 ABAQUS Numerical Modeling Techniques

2.5.1 Background Information

Various approximate methods exist when evaluating boundary value problems. The finite element method, FEM, is one such solution technique developed through the theory of virtual work. FEM utilizes variant methods to develop a stable solution to boundary value problems by minimizing Ritz based error functions. Conventional discontinuity model methodology requires that discretization of a model must conform to all geometric discontinuities. High mesh refinement is also required for adequate modeling of high stress singularity values located at discontinuities such as a crack tip.

Further manipulation of model discretization is needed when modeling crack propagation by traditional FEM techniques. Due to the requirement that all discontinuity be captured within discretization of the geometry; the mesh must mimic delamination of the material throughout the simulation. This requires that constant remeshing of the geometry is conducted throughout the analysis to capture crack growth. Crack development due to some failure modes, primarily Mode I, where crack directionality is easily determined, may be easily predictable and reproducible through this methodology. Effects of crack curvature and localized effects on crack development can be difficult to capture. Analyses of complex crack extension such as mixed mode loading effects are tedious through conventional FEM. Large computational time and the need for continuous remeshing algorithms make traditional modeling techniques objectionable for modeling processes within this research project.

2.5.2 Extended Finite Element Modeling

Alleviation of expensive computation efforts to model geometric discontinues was achieved in 1999 with the introduction of extended finite element modeling, XFEM (Simulia 2012). Development of this modeling scheme maintained traditional FEM theory while integrating local enrichment functions into crack modeling. Three techniques within XFEM have been proposed to assess cracking within model geometries: node enrichment functions, cohesive segment, and linear elastic fracture mechanics; LEFM. Each modeling technique lends itself most notably to a particular area of crack modeling.

Node Enrichment Functions

Enhancements of displacement approximations facilitate crack modeling through the introduction of two primary enrichment functions. The displacement approximation function used within XFEM analyses is given in the following equation:

$$u = \sum_{I=1}^{N} N_I(x)[u_I + H(x)a_I + \sum_{\alpha=1}^{4} F_\alpha(x)b_I^\alpha] \quad (4)$$

where u is the displacement vector and $N_I(x)$ is the nodal shape functions. The traditional FEM nodal displacement vector is denoted by u_I while a_I is the enriched nodal degree of freedom vector associated with the discontinuous jump function; H(x). Final terms in this equation denote the enriched nodal degree of freedom correlated to the crack tip. These terms are the nodal enriched degree of freedom vector; b_I^α, and the elastic asymptotic crack-tip function; $F_\alpha(x)$ (Simulia 2012).

Discontinuities caused by the presence of cracks are accounted for through the introduction of a Heavyside discontinuity jump function; H(x). Use of this step function monitors discontinuities within a model between the two faces of a crack. The nodal values of H(x), either ±1, are determined by assessing the distance of a Gauss Point to the crack plane.

$$H(x) = \begin{Bmatrix} 1 & if\ (\boldsymbol{x} - \boldsymbol{x}^{*}) * \boldsymbol{n}\ \geq 0 \\ -1 & otherwise \end{Bmatrix} \tag{5}$$

The variable x denotes the Gauss Point and x^* defines the closest location on the crack plane to the Gauss Point. The unit vector directed outward from x and normal to the crack plane at x^* is given as n is the above equation.

Singularity effects due to the crack tip are approximated through use of the elastic asymptotic crack-tip function; $F_\alpha(x)$. Four equations modeling elastic crack-tip effects are contained within F_α. Polar coordinates, shown below, are used to assess the radius and angle of the crack tip from a known Gauss point. From this function, improved accuracy of the singularity effects of the crack tip is available.

$$F_\alpha(x) = \left[\sqrt{r}\sin\frac{\theta}{2}\sqrt{r}\cos\frac{\theta}{2}\sqrt{r}\sin\theta\sin\frac{\theta}{2}\sqrt{r}\sin\theta\cos\frac{\theta}{2}\right] \tag{6}$$

In this equation, r is the radial distance and θ is the polar angle.

Utilization of the H(x) and F_α equations causes additional degrees of freedom to be applied to those nodes affected by the presence of the crack. Conventional finite element DOF’s are applied to all nodes within the finite element model. Nodes affected by the crack faces contain the enriched degrees of freedom; a_I, associated with the Heavyside step function. Degrees of freedom linked to the crack-tip functions; $b_{I,}$ are applied to nodes whose shape function is interrupted due to the presence of the crack tip. In some cases all three types of DOF’s can be applied to one node.

Accurately assessing the status of material cracking through this method requires continuous knowledge of the crack tip location, and propagation pattern. The use of F_α to monitor the crack tip singularity requires the knowledge of the crack propagation throughout the entire analysis. Due to the large computational effort in assessing the crack tip location, use of the node enrichment technique is only recommended for use in monitoring stationary crack effects. (Simulia 2012) For the analysis of crack propagation, use of this method results in a large computation cost.

To decrease computational efforts, the enriched crack-tip equation and associated DOF's are ignored in analyses associated with crack propagation. However, with this increased modeling efficiency, crack propagation must occur through an entire element so as to avoid the need to model the F_α functions. Two methodologies exist in the XFEM analysis to assess crack propagation: Cohesive Segments and Linear Elastic Fracture Mechanics.

Cohesive Segment Method

One technique for the analysis of both crack initiation and propagation can be modeled through use of a traction separation cohesive behavior definition. Within this process the path of both crack instigation and growth occur along an arbitrary and solution-dependent path (Simulia 2012). Enrichment of nodes affected by discontinuity effects are still considered in this method in a similar way to that presented earlier. However, with the removal of asymptotic crack-tip functions from the displacement approximation function, only the Heavyside step functions enrich nodes that the crack interior affects. Therefore, the approximation function reduces to the following expression:

$$\boldsymbol{u} = \sum_{I=1}^{N} N_I(x)[\boldsymbol{u}_I + H(x)\boldsymbol{a}_I] \quad (7)$$

To represent the discontinuity in the model material "phantom nodes" are superimposed over elements cracked due to crack propagation. Absence of a crack profile within an element results in phantom nodes restrained completely by the corresponding "real" nodes. With the introduction of a crack profile acting through an element, separation of the phantom and real nodes begins to occur. With the separation comes the enrichment of the element into two cracked elements through a defined traction separation law. Fully cracked elements are comprised of a mixture of both phantom and real nodes. Therefore, once an element is fully cracked, real nodes initially within the same element have the ability to move independent of each other (Simulia 2012). With the onset of crack propagation through an element, enhancement of the elemental nodes occurs with the introduction of Heavyside DOF's as discussed earlier.

Use of traction separation laws are the primary methodology used to develop crack initiation and propagation within this modeling technique. Initiation of cracking within a simulation is determined based on a defined damage criterion. These criterions specify the maximum traction that the element can sustain. When the specified traction within the analysis model exceeds the predetermined maximum value, separation of the element begins to occur based on a separation law (Simulia 2012). Traction separation can be specified in ABAQUS 6.12 for the following criterion:

- Maximum Principal Stress
- Maximum Principal Strain
- Maximum Nominal Stress
- Maximum Nominal Strain
- Quadratic Traction-Interaction
- Quadratic Separation-Interaction

Once the traction parameter has been exceeded, the ability for the material within the failing element to support the applied traction decreases due to a user defined degradation model. As separation of the real nodes reach a critical separation displacement, full elemental failure occurs, and the one element splits into two cracked elements. Instantaneous loss of an element to support a load is not supported within ABAQUS 6.12. Available linear and non-linear damage models, shown in Figure 2-12, are applied to model the traction-separation response of the material (Simulia 2012). According to the selected damage model, as the separation of the phantom and real nodes increase, the ability for the element to support the load is reduced until the separation is such that complete failure is said to occur.

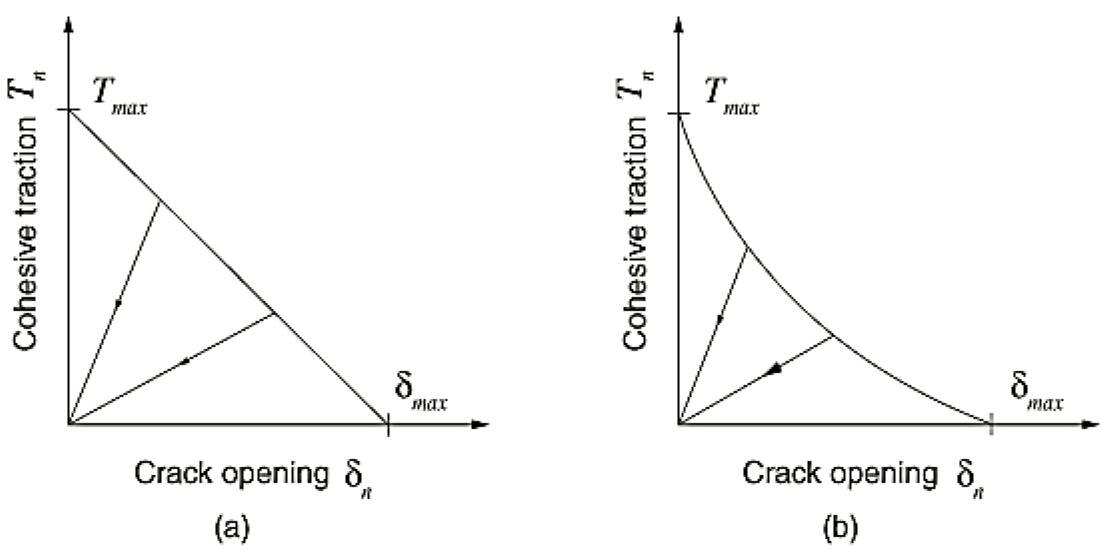

Figure 2-12: Damage Traction Separation Laws (Simulia 2012)

This generalized model has been noted to be effective in the analysis of both brittle and ductile material failures (Simulia 2012). Most notably, this procedure is most effective in modeling material fracture due to the application of a static load. As load is applied to model geometry and traction components exceed maximum sustainable values, the material will begin to fail due to fracturing of material.

Linear Elastic Fracture Mechanics Method

When the loading application occurs in an oscillatory or cyclical fashion, material failure occurs over time as the result of material fatigue. Modeling crack propagation by the cohesive segment traction and damage separation laws discussed above does not address time dependent effects on material characteristics. Instead, the theory of linear elastic fracture mechanics; LEFM, can be applied to model crack propagation for fatigue scenarios. Similar to the cohesive segment approach, computational cost is minimized in the LEFM method by only applying enriched degrees of freedom due to the H(x) jump functions. Likewise, consideration of the asymptotic crack-tip function is not considered in this method. This constraint of the modeling method therefore requires that crack propagation occurs through an entire element (Simulia 2012).

An approach akin to the cohesive segment modeling technique is applied for LEFM crack modeling. Phantom nodes are introduced into the model and separate from the real nodes when a specified damage criterion has been met. Linear elastic fracture criterion rely on the computation of relative strain energy release rates; G, at the crack tip. Strain energy release rate parameters are akin to the stress intensity factors used within the Paris Law theory. As with the stress intensity factors previously discussed, loading modes affect the value of the strain energy release rate values. Conversion between G and K values for all three loading modes is possible through the following equations (Yue 2009);

$$G_I = \frac{{K_I}^2(1-\nu^2)}{E} \tag{8}$$

$$G_{II} = \frac{{K_{II}}^2(1-\nu^2)}{E} \tag{9}$$

$$G_{III} = \frac{{K_{III}}^2}{2\mu} \tag{10}$$

where K_I, K_{II}, K_{III} denote the stress intensity factor for each mode. Poisson's ratio is denoted by ν and μ represents that shear modulus of the material. For simulation of the LEFM, models must satisfy both a crack onset and propagation criterion before extension of the crack plane will result. Onset of fatigue crack growth is determined by insuring that the following criterion is satisfied:

$$f = \frac{N}{c_1 \Delta G^{c_2}} \geq 1 \tag{11}$$

The variable N denotes the number of cycles applied to the simulation at a specified discrete time step, while ΔG is the equivalent alternating strain energy release computed for a given element. The ΔG value is determined by a specified combination of the three loading mode ΔG values. User defined variables c_1 and c_2 are associated with AASHTO S-N curve parameters. Therefore, initiation of fatigue cracking in a singular element is identified by the specification of the fatigue resilience of the material. The parameters associated with this material characteristic are derived from the AASHTO S-N curves for monitoring crack initiation. Initial determination of the fatigue category of the model geometry is important in correctly defining the crack initiation parameters. Once a specified AASHTO detail category for load-induced fatigue has been determined, numerical variables correlating to the slope and intercept of the S-N curve are applied to the model. Throughout the simulation, the number of cyclical loadings to initiate fatigue failure in an element is linked to these specified parameters.

Once it is determined that the initiation parameters are met, analysis of crack propagation is modeled using the Paris Law principles through the following criterion:

$$\frac{da}{dN} = c_3 \Delta G^{c_4} \tag{12}$$

The instantaneous rate of crack growth is noted by da/dN. ΔG denotes the equivalent alternating strain energy release rate for the material. User defined variables c_3 and c_4 correlate to the Paris Law constant terms; C and m. These variables are applied to the simulation model to facilitate the rate at which crack propagation will occur. Provided that both criterion are met, crack extension progresses a minimum of one element ahead of the current crack tip location for a specified number of loading cycles; ΔN.

2.5.3 Material Failure Criterion

Crack onset and propagation criterion are based in part on the alternating strain energy release rate values calculated due to the presence of the crack. Effects of multi-mode loadings can add difficulty in assessing the equivalent G and ΔG values within the model. Three primary methodologies within ABAQUS XFEM are used to identify G_{equiv} and ΔG_{equiv} due to fatigue loading effects. Defined approaches of fatigue failure can be specified by the Benzeggagh-Kenane (BK), Power Law, or Reeder mixed mode failure models. All three techniques assess the equivalent mixed mode strain energy release rate, expressed as G_{equiv}, throughout each loading cycle.

Benzeggagh and Kenane defined a formula for the interaction of mixed mode strain energy release rates compared to Mode I and Mode II critical failure values (Simulia 2012). Resulting strain energy release rate values for all failure modes are applied to the following equation to determine the equivalent critical G value action on the material.

$$G_{equivC} = G_{IC} + (G_{IIC} - G_{IC})\left(\frac{G_{II}+G_{III}}{G_I+G_{III}+G_{III}}\right)^{\eta} \tag{13}$$

Within this equation, G_{IC} and G_{IIC} denote critical values of Mode I and Mode II strain energy release rates. G_I, G_{II}, and G_{III} variables correlate to the computed strain energy release rate values for all loading modes as the material is loaded. The user defined exponential constant; η, specifies the degree of effect that the ratio of the computed G values has on the G_{equivC} value.

Consideration within the Benzeggagh and Kenane (BK) model is restricted to critical values of modes I and II. Effects due to critical anti-plane shearing values in this model are not included. Therefore, the use of the BK model is not appropriate for use in this research and will not be address further in this report. The other two models; Power and Reeder, both model the effects pure and mixed mode possibilities for all three loading modes.

The Reeder theory is an extension of the BK model used to asses crack propagation due to all three failure modes. This model is best used if the critical G for Mode III is not equal to that of Mode II as the model reduces to the BK law when these two G_C values are equivalent. The Reeder model was obtained out of the BK model due to its ability to effectively model loadings leading to in-plane crack development; Mode I and Mode II loading scenarios. As both Mode II and Mode III cracking are a result of shearing effects it was assumed that the equation to define Mode III failure would be directly akin to that of Mode II loading in the BK model (Reeder 1992). A linear relationship was assumed between all failure modes, the final failure criterion equation shown below was developed.

$$\frac{G_{equiv}}{G_{equivC}} = \frac{G_T}{G_{IC}+(G_{IIC}-G_{IC})\left(\frac{G_{II}+G_{III}}{G_T}\right)^{\eta}+(G_{IIIC}-G_{IIC})\frac{G_{III}}{G_{II}+G_{III}}\left(\frac{G_{II}+G_{III}}{G_T}\right)^{\eta}} \tag{14}$$

G_{IC}, G_{IIC}, and G_{IIIC} are the critical strain energy release rates of the material, and η is an equation constant used to fit the criteria to experimental data. G_I, G_{II}, G_{III} are resulting strain energy release rate values developed as the material is loaded. G_T is the sum of the G components for Mode I and Mode II; $G_T = G_I + G_{II}$ (Reeder 1992).

The Power Law described by Wu in 1965 observes the mode effects individually in the assessment of the G_{equiv}/G_{equivC} ratio. If this ratio is greater than unity, crack initiation will occur. As can be seen below, the equation relies on the determination of exponential values in addition to critical strain energy release rate values for each failure mode.

$$\frac{G_{equiv}}{G_{equivC}} = \left(\frac{G_I}{G_{IC}}\right)^{a_m} + \left(\frac{G_{II}}{G_{IIC}}\right)^{a_n} + \left(\frac{G_{III}}{G_{IIIC}}\right)^{a_o} \tag{15}$$

Development of the exponential terms is conducted through calibration of the model from experimental results. However, a linear relationship between the three contributing modes is often applied in order to “reduce the burden of experimentation” (Barbero 2013). While other exponential values are possible, linear relationships are accomplished by setting the exponents to the same value, often of unity.

2.5.4 Cyclic Simulations

Cyclical loading scenarios such as those experienced through out-of-plane distortion-induced fatigue can be modeled with the LEFM ABAQUS XFEM approach and high cycle loading scenarios. This method alters the finite element displacement equation presented earlier so as to describe the structural response due to cyclical loading events. Nodal displacement equations applied during this approach incorporate periodic displacement response through the use of truncated Fourier series. The elastic stiffness matrix continually serves as the Jacobian matrix throughout the analysis, relieving the need to solve the nonlinear equations through full Newtonian approach (Simulia 2012).

The response of a model under this loading application is achieved by first evaluating the response of the material at discrete time points throughout the analysis. Extrapolation of this response is then applied to anticipate what the response of the material over the following time increment. This increment spans ΔN number of loading cycles. In this manner crack growth can be continually updated throughout the analysis at each discrete time step (Simulia 2012). LEFM can be used within the cyclic loading approach to anticipate progressive damage within a material. Therefore, crack growth responses due to loading applications can be specified to correlate to the onset and propagation criterion previously discussed for LEFM applications.

2.6 Literature Review Summary

From the literature review it was determined that the best course of action for modeling distortion-induced fatigue was to focus on the localized connection detail and not a global scale bridge superstructure. Simulation of a multitude of stress ranges acting on web gap lengths should be run to observe the fatigue resistance sensitivity of web gap regions. Application of this analysis allows for the determination if consideration to web gap lengths should be given when contemplating rehabilitation operations.

Distortion of the transverse stiffener has been noted to be caused by multi-mode effects due to nominal and bending stresses developing in the web gap region. Knowledge of the interaction between these two failure modes is essential in determining the response of material to fatigue loading. Validation of modeling parameters therefore must be performed against experimental results of Mode I and Mode III failure in structural material used in bridge superstructures.

Fatigue detail classification of transverse stiffeners has been noted in AASHTO design specifications as a category C detail. When modeling transverse stiffener fatigue cracking, differential displacement magnitudes were therefore induced to develop in-plane stress range levels consistent with those acceptable for this detail category. Stress range levels were chosen to reflect magnitudes bounding the CAFL of category C details: 69 MPa (10 ksi). Loading was also applied to result in stresses slightly over the infinite fatigue life limit state.

Research also suggests that softening of the connection detail attenuates crack growth. Slowing of crack propagation was noted once crack lengths reached regions of low stress zones. It was hypothesized that manual horizontal extension of a crack plane may aid in precipitating the end of crack growth. Crack pathways were seen to propagate along vertical stiffener welds, into the web plate, and even into flange weld interfaces. Given this variation in crack growth, if manual direction of the crack was applied, determination and prediction of crack behavior may be more readily predictable. In order to test this hypothesis, model geometries were developed with varying horizontal crack lengths. These lengths were determined to model a small initial flaw, a theoretical thumbnail crack profile, and an extended crack length.

Tools available in ABAQUS software to monitor fatigue crack growth offer a means for modeling distortion fatigue. Literature review of this software suggests that LEFM principles can be applied to the simulation software to assess crack growth for high cycle fatigue scenarios. Crack propagation rates within available software are based on Paris Law theory. Validation of the software against multi-mode failures is necessary to ensure Paris Law growth rates can adequately predict multi-mode loading effects. Power law criterion used to determine equivalent G values was used for this analysis. The Reeder criterion were largely developed for Mode I and II failures, and there was concern that Mode III effects would not be adequately evaluated if this criterion was selected for use.

CHAPTER 3

PUBLICATION

3.1 Research Overview

Out-of-plane distortion of transverse cross bracing systems in bridge superstructures has been known to cause localized fatigue cracking. The cracking is a result of differential displacement of adjacent bridge girders, which causes high stress concentrations in unstiffened web gap regions at the interface of girder and stiffener connection plates. Fatigue cracking within the web gap can occur due to cyclical loading scenarios. Rehabilitation efforts have shown to be unpredictable in preventing crack propagation once through-thickness crack profiles have developed (Mahmoud, Meagher and Yen 2006). Therefore, understanding the mechanisms causing fatigue crack propagation in such detail is essential in developing effective repair methods. In this study, numerical analyses of typical web gap connections are conducted using the Extended Finite Element Method to characterize crack directionality and growth rate. Simulations varying the web gap length, stress range, loading ratio, and initial crack length were used to determine the primary variables effecting crack growth in the web gap region. Increasing the web gap length was noted to stabilize crack propagation rates resulting in stable growth, which can be correlated to the Paris Law. Elongation of horizontal initial crack lengths resulted in reorientation of crack growth. In stiffer web gaps, a combined high stress ratio and long initial crack length resulted in crack profiles propagating into the flange-web interface with eventual crack arrestment. The study suggests that horizontal extension of initial cracks has the potential to cause the crack to arrest, after stable propagation, without adversely compromising local structural integrity of bridge superstructures.

3.2 Introduction

Throughout the service life of a bridge, cyclical loadings have the ability to produce fatigue cracks at critical connection details. Multi-girder steel bridge systems designed with transverse cross bracings can be especially prone to distortion fatigue cracking. The interaction of transverse stiffeners on bridge girder members is a primary interface facilitating cracking. Conventional union of cross bracing to bridge girders is commonly achieved through the use of connection plates welded to the girder web. Until the 1980's, welding of connection plates to bridge tension flanges was specifically avoided. Instead, the plates were cut short of the girder flanges introducing an inherent unstiffened gap in the bridge girder web (Fisher and Keating 1989). Differential displacements of bridge girders can result in out-of-plane distortion of the connection leading to high stress levels localized in the unstiffened web gap. Crack initiation due to distortion at the web gap normally occurs within the first decade of service (Fisher and Keating 1989). Current AASHTO LRFD bridge design codes provide specifications that ensure adequate fatigue life as a preventative measure against crack initiation for newly designed structures. This is achieved through positive welding of the stiffener to the girder flange. However, a predicted 85% of operational bridges still contain fatigue prone web gap details (Altay, et al. 2003).

Elongation of the web gap region has been shown to decrease stress concentrations within the unstiffened girder region. Variation in the web gap length was found to do little to attenuate localized deformation magnitudes due to the differential girder displacement. However, the reduction in stress concentration due to a lengthened web gap may result in arrestment of fatigue crack growth after initiation has occurred (Castiglioni, Fisher and Yen 1988). While a correlation exists for an increase in fatigue strength due to a longer web gap, a direct proportionality has yet to be found. Previous studies noted erratic behavior in short web gap regions under cyclical displacements. Unpredictable results were noted for web gaps of lengths less than five times the web thickness (Bowman, et al. 2012).

Estimations have been made that 90% of all fatigue cracking may be related to out-of-plane distortion or secondary stresses at fatigue critical details (Connor and Fisher 2006). Since the 1960's addition of fatigue life considerations within AASHTO Bridge Design Guide Specifications has provided a preventative measure against crack formation from fatigue loading scenarios. S-N fatigue curves provide assurance that stress levels at fatigue critical details do not adversely affect bridge serviceability. However, minimal guidance is provided to assist with rehabilitation of the superstructure after a fatigue crack has developed. Initiation of fatigue cracks in the web gap regions for structures not designed to current code specifications is anticipated to occur within 1/5th of the design service life of a bridge (Fisher and Keating 1989).

The lack of evaluation guidelines offer avenues in which improvements can be made to damage assessment. In-field instrumentation and monitoring have long been viewed as effective tools for fatigue evaluation. An inspection frequency not exceeding twenty-four months is recommended by the Federal Highway Administration (Federal Register Rules and Regulations 2004). Frequent assessment allows for constant observation of those members and connections which may be considered fracture critical. Despite these precautionary measures, some cracking may go undetected due to the difficulty associated with monitoring and adequately instrumenting members in bridge superstructures. Application of numerical modeling techniques may be useful to identify fatigue-prone details. Modeling may offer a unique perspective to analyze stress concentrations, distortion effects, and fatigue crack propagation caused by cyclical loadings. Utilization of ABAQUS Extended Finite Element Method software; ABAQUS XFEM (Simulia

2012) offers the ability to monitor fatigue loading effects in a unique manner. Crack propagation can be monitored throughout a simulation to observe the effects of distortion when the directionality of crack propagation may not be initially known.

This study was conducted to evaluate the effect of stress range magnitudes within the web gap, the web gap size, and the initial crack length, on the propagation of cracks due to out-of-plane distortion. Prior to conducting the simulations, the viability of ABAQUS XFEM software to model high cycle fatigue crack growth was assessed. Evaluation of software capabilities was conducted to ensure adequate correlation with experimental testing of fatigue crack growth for Mode I and mixed mode loading scenarios. Such assessment required the evaluation of utilizing the Paris Law for modeling crack propagation under Mode III loading. Experimental data was used to validate the modeling approach. Use of the Paris Law under Mode III dominated mix-mode loading scenarios was also validated from experimental data. The culmination of this research modeled propagation of cracks initiating within transverse connection plate web gap regions. Analyses of three web gap lengths were conducted with initial horizontal crack profiles ranging in magnitude. Differential displacements and stress ratios were applied to models to simulate adjacent girder displacement effects.

3.3 Methodology

It has been noted that fatigue of transverse connection plates welded to girder webs is induced by multi-mode failure acting on the steel material (Fu, et al. n.d.). As the connection is distorted due to girder differential displacement, nominal and out-of-plane bending stresses are developed in the web gap. Crack development under a mixed Mode I/Mode III mechanisms results from a combination of shear stresses acting parallel to the plane of the crack and normal tensile stresses acting perpendicular to the crack face. This is characteristic to stresses found within the web face of the transverse girder connection. Figure 3-1 illustrates the localized distortion of the web gap and the stresses induced in this region

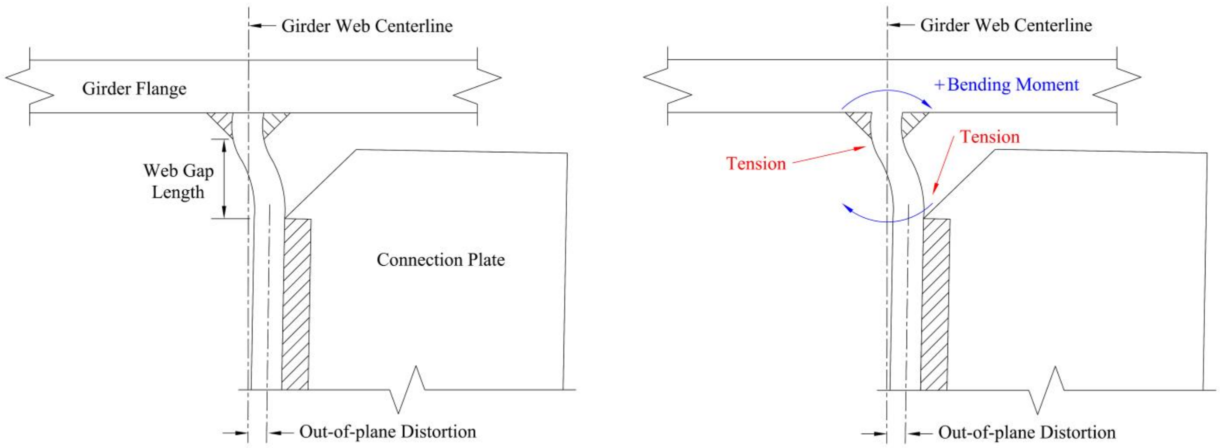

Figure 3-1: Distortion of Girder Diaphragm Connection (Fu, et al. n.d.)

In order to successfully simulate fatigue crack propagation it is imperative that an understanding of steel behavior under Mode I and Mode III failure is obtained. Consequently, validation studies of the ABAQUS XFEM software were conducted to ensure adequate results could be obtained when simulating fatigue cracking of steel under these two modes of failure.

Utilization of ABAQUS XFEM software provides a new means by which crack modeling is possible. Traditional FEM approach to model discontinuities requires that model discretization conform to all discontinuities present in the geometry. Therefore, modeling of crack growth requires remeshing algorithms to ensure continuity. Primary significance of the ABAQUS XFEM software decreases the computational effort required to model discontinuities by applying localized enrichment functions to nodes only affected by the crack plane. Elements determined to be affected by the presence of the crack plane are superimposed with phantom nodes which are activated once the crack plane extends through the elemental volume. This activation allows for simulation of crack elongation on an elemental level of the discretized region. Fully cracked elements are comprised of a combination of phantom and real nodes.

Separation laws applied to models under fatigue loadings are determined through the use of linear elastic fracture mechanics; LEFM. Two criteria must be met before fatigue cracking may progress. The first criteria, shown below, assesses onset of crack growth insures that the following criterion is satisfied;

$$f = \frac{N}{c_1 \Delta G^{c_2}} \geq 1 \tag{16}$$

where c_1 and c_2 are user defined variables describing the fatigue resistance of the geometry in question. The variable, N, denotes the number of loading cycles applied to the geometry and ΔG is the equivalent strain energy release rate of an element considering all loading mode effects. The second failure criterion determines the rate that the crack plane propagates through the material. This criterion, based on the Paris Law growth theory, is shown below.

$$\frac{da}{dN} = c_3 \Delta G^{c_4} \tag{17}$$

where c_3 and c_4 correspond to the Paris Law constants C and m, respectively. Material failure criterion are assessed based on an equivalent strain energy release rate; G_{equiv}. This variable is determined by relating the strain energy release rates of the three primary failure modes through a power law relation, which determines the contribution of every mode to crack propagation (Simulia 2012).

$$\frac{G_{equiv}}{G_{equivC}} = \left(\frac{G_I}{G_{IC}}\right)^{a_m} + \left(\frac{G_{II}}{G_{IIC}}\right)^{a_n} + \left(\frac{G_{III}}{G_{IIIC}}\right)^{a_o} \tag{18}$$

Critical values of the strain energy release rate for each mode are determined by the user defined G_{IC} G_{IIC}, and G_{IIIC}. User defined variables; α_m, α_n, α_o determine the weight of a specific mode type on the equivalent strain energy release rate values. Values for α_m, α_n, and α_o are determined by calibrating the power law relation to experimental data. Cracking of the material will occur if ΔG_{equiv} values are above the threshold value (ΔG_{th}), and maximum G values do not exceed the critical value (G_C). The variables ΔG_{th} and G_C are user defined constants specified within material failure criterion properties.

High cycle fatigue scenarios can be modeled using cyclical loading applications available in ABAQUS to extrapolate damage effects over an extensive number of cycles. Propagation of damage is modeled by the analysis of material damage response at discrete time intervals. Extrapolation of this damage is used to assess material response at each successive discrete time step. Combined with a user defined crack propagation rate, assessment of the material and predicted damage development is made. If applicable with user defined failure criterion, crack elongation will occur within the simulation at these discrete time steps.

Data taken from modeling scenarios consisted of load cycle numbers, fatigue crack lengths, and strain energy release rate values. Results of modeling scenarios were assessed against the following criteria that served to determine viability of the software to model fatigue crack propagation.

- Ability for numerical assessment to simulate high cycle fatigue scenarios
- Capability of numerical methods to track crack propagation through cyclical loadings
- Facilitation of user defined critical strain release rate parameters for test material
- Observation of convergence within results through mesh refinement studies

- Comparison of theoretical mathematical modeling techniques against results
- Acceptable results compared to experimental fatigue test data

3.4 Mode I Validation

Initial validation studies utilized experimental fatigue results of uniaxial tension tests corresponding to a purely Mode I failure mechanism (Klingerman and Fisher 1973). Testing consisted of fatigue loading on 254mm long, 95.25mm wide by 6.35mm thick (10" x 3¾"x ¼") A36 rolled steel plates. A 3.18mm, ⅛", diameter hole located at the center of the specimen geometry served as the location for a horizontal notch to be placed in the plate. This cut served as the initial location for crack propagation throughout the experiment. Two experimental uniaxial tests with varying initial crack lengths and loading ranges were used for model verification. The first test; CP_23, consisted of a plate with a 5.23mm (0.207") initial half crack length and 37.37 kN (8.40 kip) loading range. The second experiment; CP_25, comprised an initial half crack length of 7.46mm (0.294") and a loading range of 27.58 kN (6.20 kips). The minimum load applied to both plates during fatigue testing was 8.89 kN (2.0 kips).

Three-dimensional finite element models of geometries corresponding to the dimensions specified above were developed using ABAQUS 6.12 software (Simulia 2012). Specimen material was modeled as linear-elastic A36 steel with a modulus of elasticity of 200 GPa (29,000 ksi) and a Poisson's ratio of 0.30. Modeling of material fatigue resistance was imputed in accordance with theoretically accepted values. ΔK_{th} and K_{IC} values were determined to be 3.63 MPa√m (3.30 ksi√in) and 50 MPa√m (45.80 ksi√in) respectively.

Linear elastic fracture mechanics (LEFM) was used throughout numerical modeling of the fatigue crack growth. Designation of material fatigue cracking behavior was defined through user inputs of material fatigue classification and crack propagation rates. Fatigue classification was applied to this research based off of AASHTO S-N fatigue design curves. Depending on the nature of the initial notch fatigue classification of the steel plates could vary widely. Therefore, multiple simulations were conducted on the models to test for acceptable category distinction. Comparison of experimental and simulation results were performed to determine appropriate fatigue classification. The rate of crack propagation was specified from the fatigue rest results of the steel panels (Klingerman and Fisher 1973). This growth rate was specified for all models simulated throughout the Mode I validation study as;

$$\frac{da}{dN} = 1.86E^{-9}\Delta K^{3.1} \tag{19}$$

where crack length is measured in millimeters and ΔK values measured in units of MPa√m. Movement of the top and bottom surfaces were restrained through rigid body constraints linked to reference nodes located at the center of the respective surface. Boundary conditions were applied to the bottom reference node to simulate a fixed connection at the bottom of the test plate. Fatigue loading was applied to the top reference node. Models were developed using eight node reduced integration continuum elements. A convergence study of the stress levels within the geometry was conducted to determine the sensitivity of the analysis to mesh density. An adequate element size was determined to be 3.18 mm (⅛”). Figure 3-2 shows the geometry of the specimen tested under Mode I (Klingerman and Fisher 1973) and the corresponding finite element model developed in this study for verification.

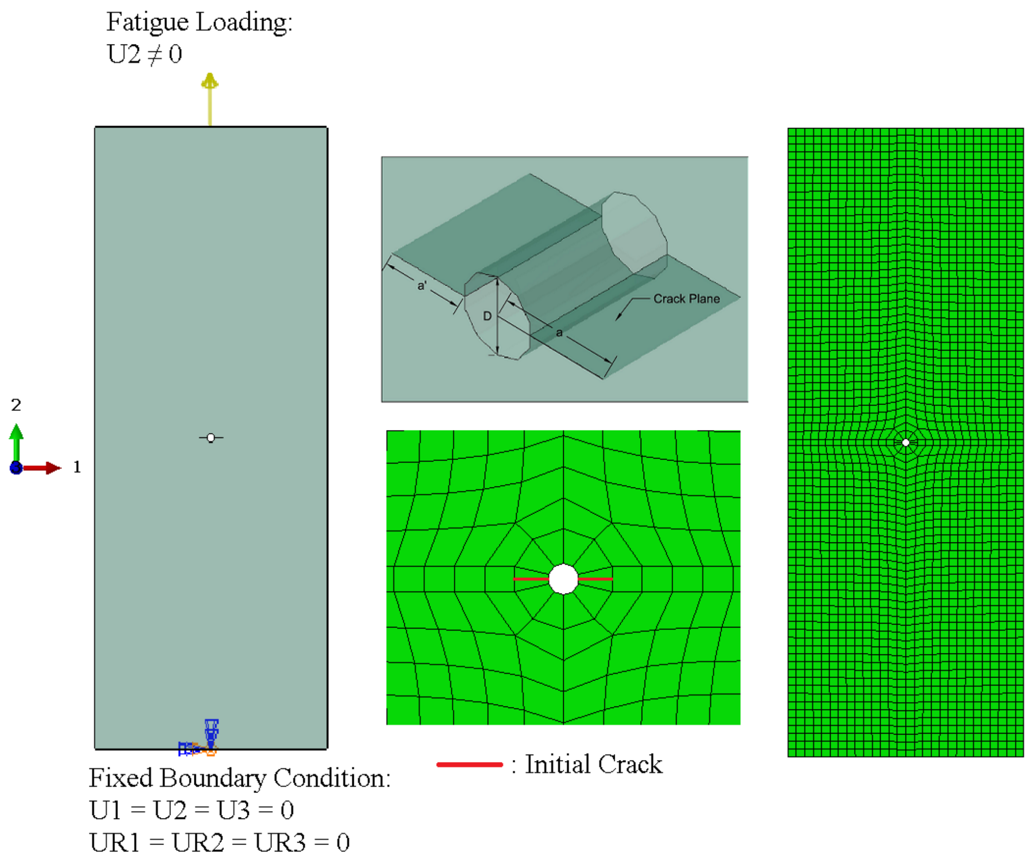

Figure 3-2: Mode I Model Development

Loads applied to the plate geometry were consistent with experimental testing procedures. An initial static load with a magnitude equal to the mean cyclical load was applied to the specimen. Cyclical loadings were induced to apply fatigue loads the test specimen over the specified load range. A plane was positioned within the geometry to serve as the location of the initial notch cut into the experimental test specimens. This plane was denoted as the initial crack location and crack growth was allowed to occur throughout the entire domain of the material. Fatigue loading simulations of the test geometry allowed for monitoring of crack propagation emanating from the initially designated crack location.

Data corresponding to the crack length versus number of cyclical loadings and the strain energy release rate were extracted from each model for post processing analysis. Increase in crack extension was noted only when the crack plane had passed through all elements within the thickness of the plate. Comparisons of crack propagation were made between experimental and modeling results. Additionally, experimental and simulation results of crack propagation rates versus the Mode I alternating stress intensity factor, ΔK_I, were compared.

Theoretical calculations of ΔK_I values were also made from crack length versus loading cycle information taken from simulation tests. The relationship of the stress range; $\Delta\sigma$, to ΔK_I for crack growth of a uniaxial tension specimen is defined by LEFM theory as

$$\Delta K_I = \sqrt{\sec\left(\frac{\pi a}{w}\right)}\sqrt{1 + \frac{D}{2a'}}(\Delta\sigma)\sqrt{\pi a} \tag{20}$$

where a is the half crack length including the hole radius, a’ is the half crack length excluding the hole radius, w is the width of the plate, and D is diameter of the central hole. Results of fatigue cracking are reported in ABAQUS XFEM software by use of the strain energy release rate. Therefore, strain energy release results from the simulations were converted into stress intensity factors for final analysis purposes as shown below.

$$G_I = \frac{{K_I}^2(1-\nu^2)}{E} \tag{21}$$

Preliminary validation studies of ABAQUS XFEM methodology in regards to Mode I fatigue loading indicated fatigue cracking of both uniaxial tension models emanating horizontally through the plate material from the machined notch. Crack extension and the correlating fatigue cycle number was recorded once the crack plane stretched across the entire thickness of the plate geometry. Comparative results of crack propagation are given in Figure 3-3 in terms of the half crack length to the number of fatigue loading cycles. The figure shows very good correlation between experimental and numerical simulations.

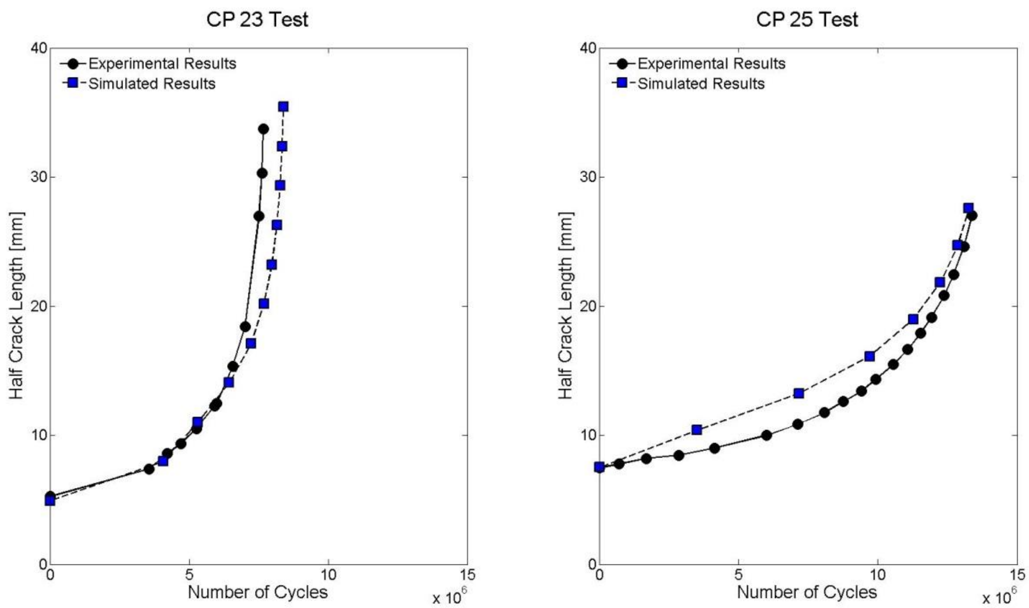

Figure 3-3: Mode I Crack Propagation Results

Crack propagation was seen to occur between 10E-8 and 10E-5 in/cycle. Alternating stress intensity values of model results were contained within the theoretically defined threshold and critical values. Results of experimental, simulated, and theoretical results are noted to all reside along the experimentally defined crack propagation rate of Mode I loadings. Maximum and minimum percent error recorded between the simulated and theoretical ΔK_I values were determined to be 26.74% and 6.58% for CP_23 models while percentage error bounds of 19.57% and 9.20% were calculated for model CP_25. Results of Mode I crack propagation in terms of da/dN growth rate compared to ΔK_I values are provided in Figure 3-4.

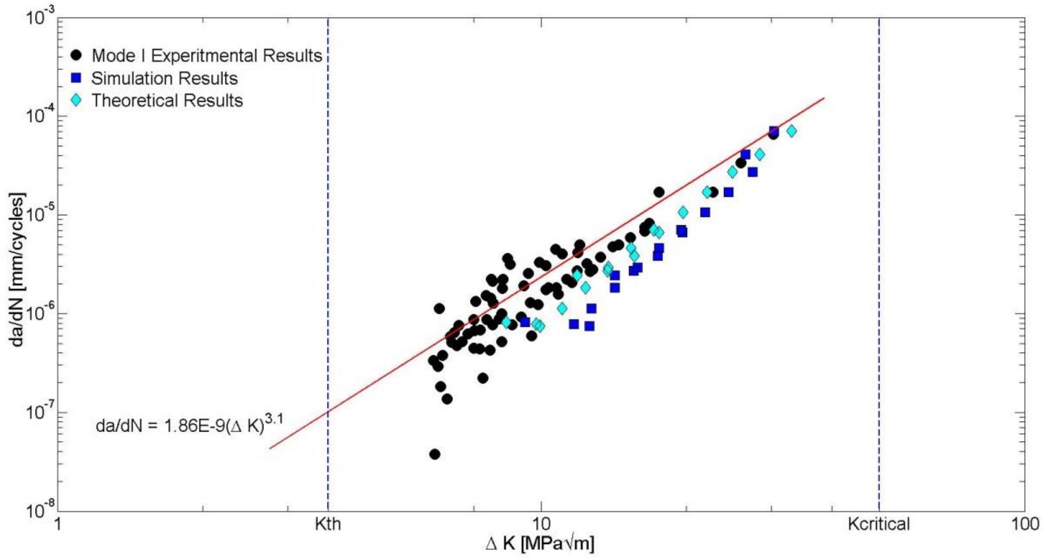

Figure 3-4: Crack Propagation Rate Results

3.5 Mode III Validation

ABAQUS fatigue modeling implements Paris Law theory to determine crack propagation rates. Development of the Paris Law was conducted from observations of Mode I experimental results. Application has therefore largely been restricted to Mode I analyses. For the purposes of this project it was essential to evaluate the Paris Law against Mode III fatigue data. While an experimental study of crack growth due to out-of-plane loading would have been ideal for validation purposes, such data did not exist at the time of the project. However, experimental testing of Mode III fatigue loadings was conducted in 1982 through torsional loading of 4340 steel samples. The results of this study illustrated that crack propagation rates of Mode III fatigue loadings could be correlated to the alternating stress intensity factor; ΔK_{III}, in the same fashion as the traditional Paris Law (Ritchie and et.al 1982). Due to the nature of the results from this experimental test program, validation studies of ABAQUS XFEM capabilities under Mode III fatigue failures were therefore conducted referencing the torsional experimental research.

Physical testing was conducted on circumferentially-notched cylindrical dog bone specimens with a 24.6mm central diameter. The dog bone specimen was 406.2 mm in length. Circumferential initial notching of the specimen was located at the center of the test geometry and served as the location of crack initiation. The circular notch plane was noted to penetrated 1.22 mm into the material. Specimens were fatigue loaded to maintain a nominal ΔK_{III} value ranging from 10 to 100 MPa√m. The loading ratio was restricted to -1.0 throughout all conducted tests.

Model geometries were developed in ABAQUS 6.12 finite element software (Simulia 2012) to capture the effects of fatigue loading on crack propagation. Simulations were conducted on geometries focused on the central portion of the test geometry. Modeling of the dog bone end sections were avoided to minimize computational time, and to allow for the effort of the simulation to be focused on the fatigue crack growth. A cylindrical area of diameter 24.61mm and length of 100mm was used to simulate the torsional test specimen. Three dimensional eight node reduced integration continuum elements were used in the simulation. Element sizing was maintained from Mode I validation tests with a length of 3.175 mm (⅛”). All elements in the model were assigned material properties consistent with linear-elastic AISI 4340 steel with a modulus of elasticity of 200 GPa (29,000 ksi) and a Poisson’s ratio of 0.30.

Fatigue resilience of the material was defined by specifying a ΔK_{th} value of 3.626 MPa√m (3.3 ksi√in) and K_C values that correlated to the three primary failure modes. With the potential for mix mode effects to take place within this analysis, a ratio of 1:0.8:0.7 for Mode I, Mode II, and Mode III K_C values was applied to the model (Jie-Oing 1989). The K_{IC} value was maintained at 50 MPa√m from the Mode I validation study. As with the Mode I validation tests, fatigue classification of the connection was thought to not be restricted to one classification type.

Therefore a parametric study was conducted on models ranging from a class A specification to a class E'. The rate of crack propagation was developed from published experimental testing results as;

$$\frac{da}{dN} = 2.36E^{-09}\Delta K^{2.79} \tag{22}$$

Crack length measurements in units of millimeters, and ΔK values in terms of MPa√m were given for the above equation (Ritchie and et.al 1982).

Cyclical fatigue loadings were applied as a rotational displacement to one end of the torsional beam while fixed boundary conditions were applied to the alternate end of the geometry. Rotational displacements were applied to induce ΔK_{III} values within the range of 10 to 100 MPa√m. Rotations were applied with an amplitude specification that ensured a stress ratio, R, of -1.0. Multiple simulations were conducted on the same geometry with varying rotational magnitudes. This was done to ensure that observations were made of cracking effects throughout the entire range of acceptable K_{III} values. Rigid body constraints were applied to the ends of the specimen to ensure that rotation was consistent throughout the cross-sectional area.

Finite difference procedures in terms of the axial torque (T), un-cracked cross-sectional length; a, and outer geometric diameter; b, were used to monitor ΔK_{III} and ensure that values stayed within the 10 to 100 MPa√m range. Theoretical calculation of ΔK values for torsional fatigued materials is based on the following equation (Ritchie and et.al 1982);

$$\Delta K_{III} = \frac{2\Delta T}{\pi a^3}\sqrt{\pi(b-a)}\,g\left(\frac{a}{b}\right) \tag{23}$$

The function g(a/b) in the above equation is a function of the ratio of the un-cracked diameter to the outer diameter of the material. The value of this function changes as crack propagation occurs and the crack length increases in magnitude. As this ratio approaches 1 the function g(a/b) also approaches unity (Ritchie and et.al 1982).

A circumferential crack plane of 1.22 mm was inserted into the model to denote initial cracking of the geometry. Crack extension was defined to occur when the crack plane cut through elements that lay in a straight line crossing the center of the cross-sectional area. Boundary conditions as well as the discretization of the test geometry are shown in Figure 3-5.

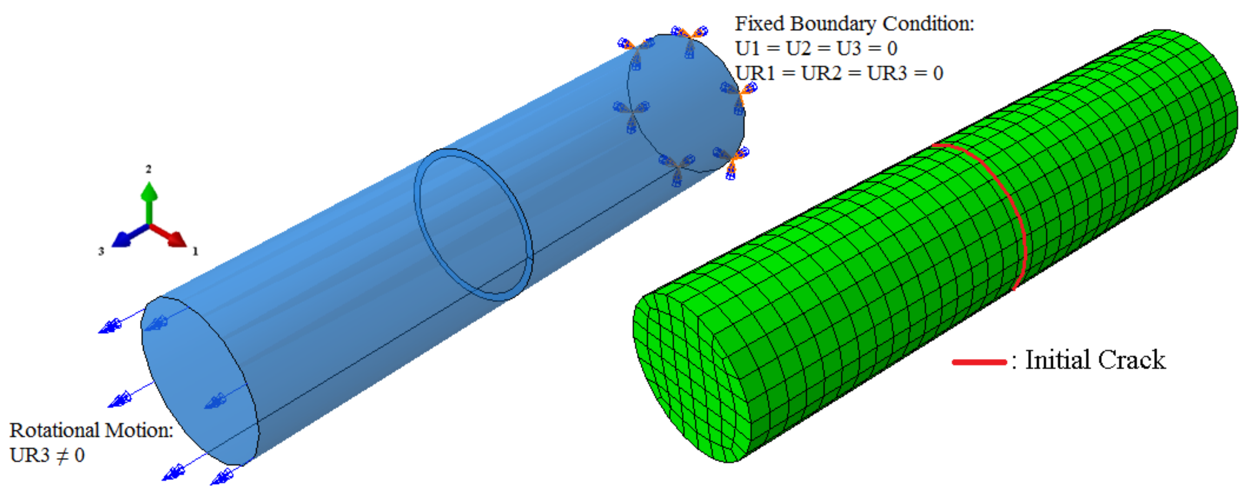

Figure 3-5: Torsional Model Development

Information corresponding to the elongation of the crack plane and the Mode III strain energy release rates were collected from the simulations. Strain energy release rate results from the simulations were converted into stress intensity factors for analysis purposes. Conversion is achieved through the following equation:

$$G_{III} = \frac{{K_{III}}^2(1+\nu)}{E} \tag{24}$$

Crack propagation rates were compared between experimental and simulated crack propagation responses. Theoretical ΔK_{III} values were also computed from crack length information obtained from simulation results. Analyses of crack propagation rates against ΔK_{III} values were conducted to ensure model inputs were responding with appropriate results.

Modeling results illustrated that fatigue cracking radiated through the test material along the central cross-sectional plane of the material. Crack propagation rates of experimental results to simulated models served as the primary variable for software validation. Results of crack propagation in Figure 3-6 illustrate da/dN growth rates with respect to ΔK_{III} values.

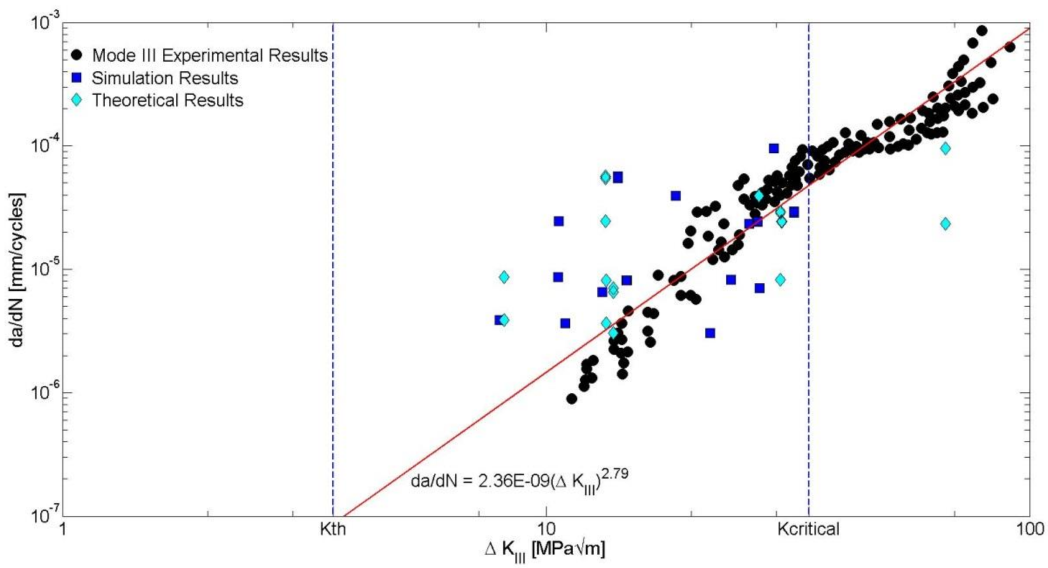

Figure 3-6: Crack Propagation Rate Results

Results of crack propagation show crack development occurring between 10E-6 and 10E-3 mm/cycles. It was also noted that crack enlargement for both experimental and simulated results were not restricted within the theoretical bounds for crack growth. Experimental ΔK_{III} values that lead to crack enlargement were however contained within the user defined bounds. While variation in the results exists, it should still be noted that crack propagation rates of the simulated fatigue crack growth were seen to align with experimental test results as shown in Figure 3-6.

3.6 Connection Geometry and Modeling Approach

Once validation of the ABAQUS software was completed for Mode I and III studies using the Paris' Law, modeling of a typical transverse connection plate was performed to predict crack propagation rate and pattern in the questionable detail. Configuration of the model was developed from the design example 2 of the American Iron and Steel Institute (1997). Geometries of girder and angles corresponded to those in the positive moment region of a two span, simply supported straight bridge profile as shown in Figure 3-7. The models consisted of two adjacent girder members with 3.048 meter; 120", spacing connected by angular cross bracing. Stiffener plates welded to the girder web were utilized to anchor the cross bracing system to the girder web. Welds were modeled between the girder and connection plate using a triangular cross-section with a throat dimension of 9.525 millimeters; 3/8". The girder depths were 0.61 meters with the transverse stiffener connection detail located in the center of the girder material. This model setup removed effects that boundary conditions would have on web gap stress levels and crack growth results based on previous experimental testing (Ghahremani, et al. 2012). Vertical symmetry of the connection was applied to the model resulting in only half of the 2 foot deep model being simulated. Symmetry constraints provided decreased computational time that was beneficial to model performance. In addition, computational cost was reduced by developing a multi-resolution model where one of the girders was modeled and connected to the other girder through a rigid surface using line elements.

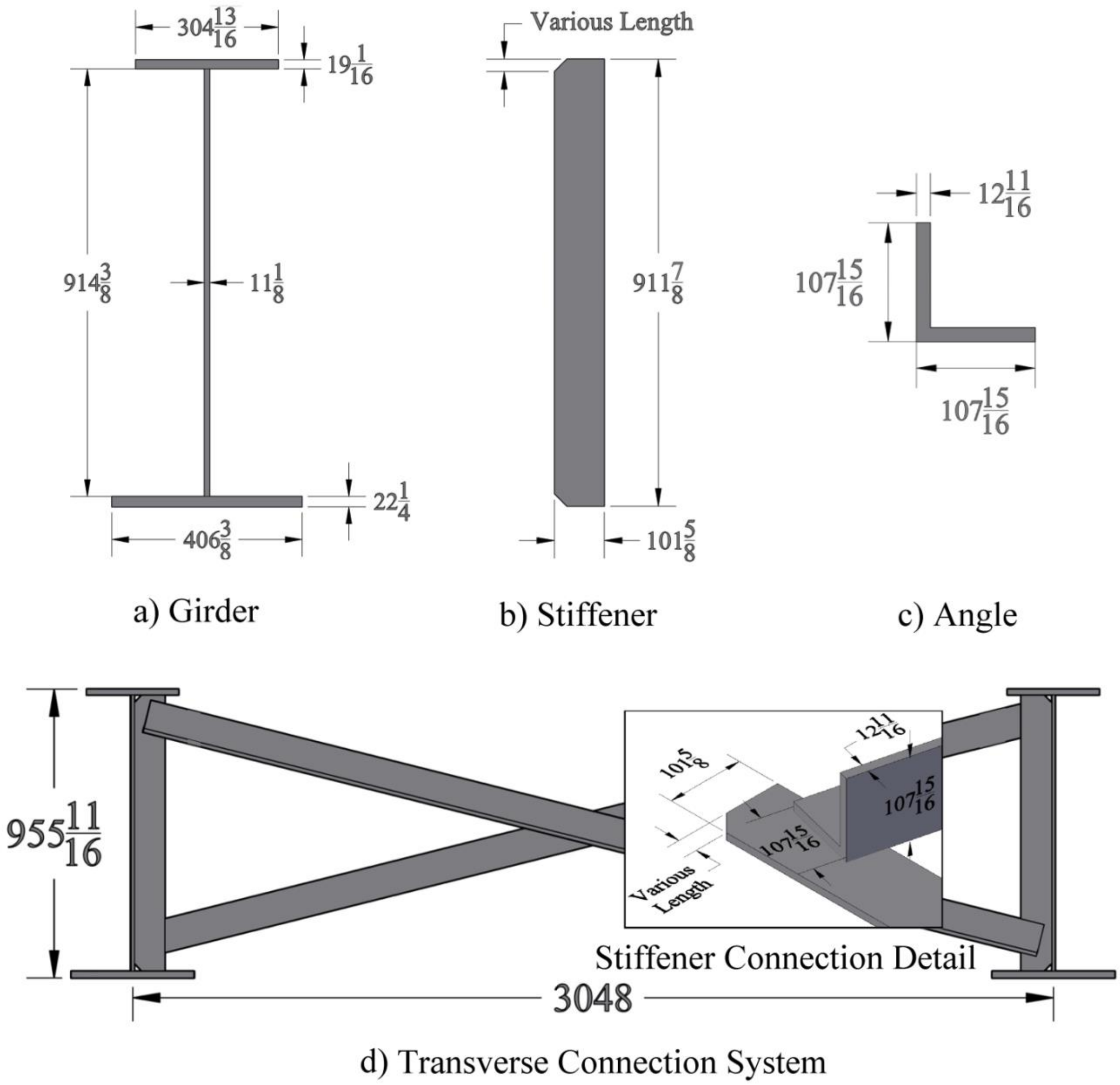

Figure 3-7: Transverse Connection Geometries [mm]

Linear elastic material properties of A36 steel was specified to all geometries within the model with modulus of elasticity and Poisson's ratio values of 200 GPa (29,000 ksi) and 0.3 respectively. Analysis of fatigue cracking was localized within one girder geometry. Three-dimensional eight node reduced integration continuum elements were used to model the girder, stiffener, and weld components in which analysis of fatigue cracking was occurring. Element length of three-dimensional elements was specified as 6.35 millimeters within these components. Two node Timoshenko linear beam elements were used to model angular cross bracing members and the girder adjacent to that undergoing fatigue crack analysis. A maximum linear element size of 0.305 meters was applied to these model geometries. Displacement of the linear girder was restricted to vertical motion which allowed for cracking in the 3D continuum model to be strictly a result of distortions caused by differential displacement. Full constraint was applied along the outside edge of the three-dimensional girder edge to mimic the constraint applied in experimental testing (Ghahremani, et al. 2012). Angular cross bracing members were connected to both girder members through kinematic coupling restraints. Modeling techniques are shown in Figure 3-8.

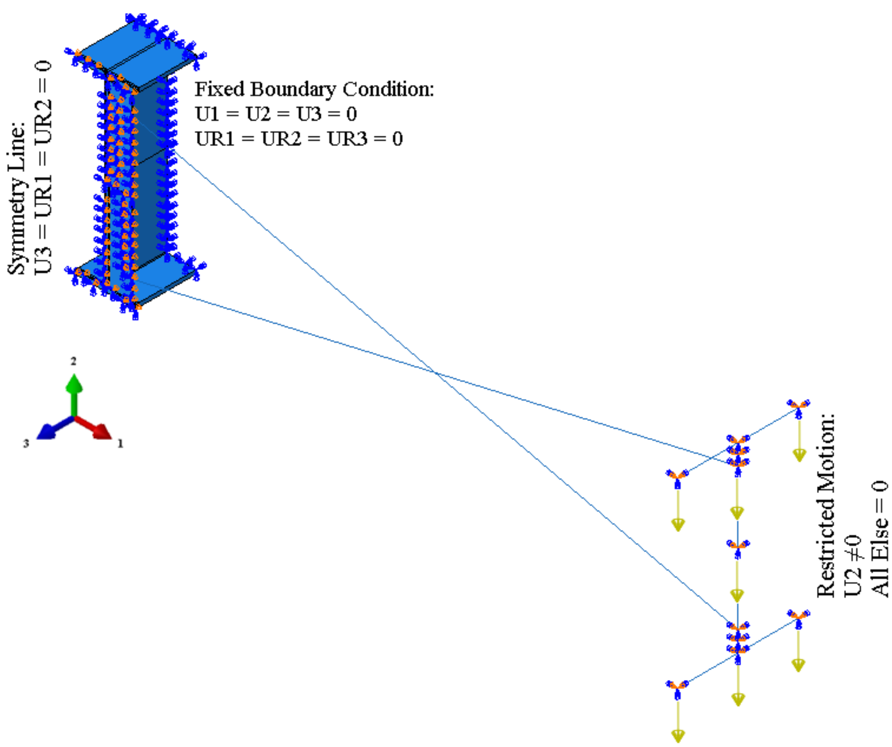

Figure 3-8: Transverse Connection Model

Fatigue sensitivity of transverse connection plates has been noted to be primarily caused by the stiffness of the connection, the loading ratio acting on the structure, and to the localized stress range concentrated within the web gap. Analysis of connection stiffness was conducted through the analysis of three web gap lengths: 25.4, 12.7, 6.35 mm. Vertical displacements were applied to the linearly modeled girder member to simulate differential girder displacement. Effects of alternating stress levels within the web gap region were analyzed by varying the magnitude of displacement applied to the model. Loading ratios; R, of 0.0 and 0.5 were used to assess the effects that complete and partial removal of the cyclical load would have on structural response.

Translation magnitudes applied to the models were determined by the stress range induced in the web gap regions. Displacements were applied that resulted in average tensile in-plane surface stress ratios of 55, 69, 83 110 MPa (8, 10, 12 and 16 ksi) within the web gap region for each loading ratio. These magnitudes were chosen to observe effects of stress ranges that bounded and exceeded the constant amplitude fatigue limit for an AASHTO category C detail.

Models were assessed on two case studies of differential displacement magnitudes. In both studies model results were analyzed to observe the directionality and rate of crack growth. Any models experiencing material yielding or fracture were disregarded as they did not conform to LEFM assumptions being utilized in this research. The first cases study analyzed models subject to displacement magnitudes that induced these stress levels within each individual web gap region. Four different displacements for each load ratio case were applied for each web gap thickness.

The second case study observe the effects that stress ranges above the category C CALF magnitude would have on the fatigue resistance of stiffer web gap regions. This study was conducted through application of additional displacement magnitudes to the stiffer web gap regions; 12.7 and 6.35 mm. For this case study models with a 6.35 mm web gap length were subjected to differential displacements equal to those applied to the 12.7 and 25.4 mm web gaps from case study one. Connections with 12.7 mm web gap lengths were subjected to a differential displacement equal to those developed for case study one analysis of 25.4 mm web gap regions.

Vertical displacements were cyclically applied to the linear element girder member for each analysis. Average daily truck traffic (ADTT) data obtained from the Colorado Department of Transportation; CDOT, and indicated that an ADTT of 1175 trucks per day could be expected to travel across a typical bridge deck (CDOT 2014). Provided this information and the knowledge that inspection intervals are a maximum of 24 months, approximately 850,000 fatigue loading cycles are predicted to occur between consecutive inspections. Each model was simulated for 10 million constant amplitude fatigue cycles to allow for analysis of crack propagation over multiple inspection intervals if no retrofit was applied to the connection. Upon the completion of the simulations, information on the crack extension and strain energy release rates was obtained from each model. This information was used to monitor crack growth for each model as well as the crack propagation rate due to the fatigue loading.

Horizontal crack planes were placed within the 3-D girder a distance of 1.27 mm away from the intersection with the connection plate in each model. Three crack profiles were tested throughout this analysis. Half crack lengths of 6.35 mm, 10.16 mm, and 17.78 mm were used for simulation purposes. These crack lengths served to model effects of several different crack length scenarios that could be present within the connection detail. A small half crack length of 6.35 mm was applied to the model to observe the effects that a small through thickness crack may play on fatigue resilience. It was hypothesized that realistic initial crack lengths occurring from only distortion effects would be twice as long as the girder thickness. This prediction steams from the theory that cracking would tend to appear first on one surface and grow through the material in a thumbnail pattern. Initiation is said to occur once the crack is a through thickness therefore at initiation the crack length will be twice the girder thickness. This correlated to a half crack length of approximately 10.16 mm. The final initial half crack length of 17.78 mm was simulated to observe the effect of the location of the initial crack on propagation direction.

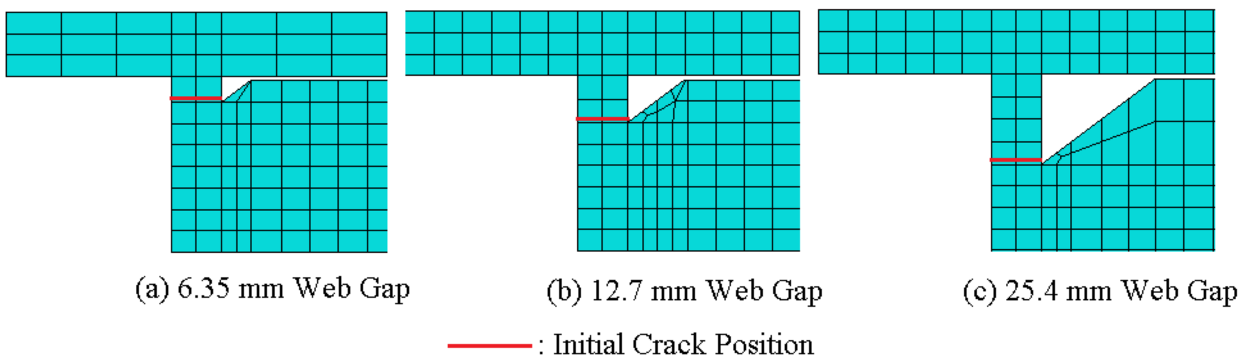

Figure 3-9: Mesh Densities

A fatigue crack propagation criteria identical to that used for Mode III fatigue validation was assigned to the models. Application of Mode III failure criteria was supported by many studies suggesting that out-of-plane distortion fatigue is dominated by Mode III loading.

3.7 Simulation Results

3.7.1 Crack growth and Propagation Rate

Initial inspection of results consisted of determining the stress ratio and maximum stress range induced in the web gap region for each displacement case. Application of LEFM requires that stress levels within the material are below yielding limits of the material; 345MPa (50 ksi) for A36 steel. Yielding was noted in models consisting of 12.7 and 6.35 mm web gaps with case two displacement values. Models of 6.35 mm web gaps yielded when displacements applied for 25.4 mm web gaps case study analyses were used. Therefore, worst case scenario analyses were only conducted using 12.7 mm web gap displacements for the smallest web gap. Yielding of 12.7 mm web gap material was only noted when 3.05 and 6.03 mm displacements were applied for case study two.

Results of transverse stiffener fatigue cracking are discussed below in terms of the crack propagation rate. Simulations that showed no sign of crack propagation over 10 million cycles were typically associated with case one loading profiles when stress ranges were near the constant amplitude fatigue loading (CAFL) levels. In other cases, higher displacement magnitudes creating high stress range levels resulted in unstable crack growth results. Classification of fracture crack growth was determined if crack growth occurred in two consecutive loading cycles. Models that experienced fracture of the connection material before fatiguing to a load cycle number of 500,000 have been referenced, but were excluded from further analysis.

Directionality of crack growth was seen to vary due to web gap length, applied differential displacement, the initial crack length, and loading ratio within each conducted simulation. Four primary crack propagation directions were noted to occur. Crack tips were seen to grow diagonally downwards through the web plate material or propagate up into the flange interface. In some cases crack profiles were seen to extend vertically down into the web and connection plate weld interface. Horizontal cracking in the web material was also noted. Classification of the direction of crack growth is noted in Table 3-1 on the following pages. It is worth noting that all of the mentioned crack propagation scenarios observed in the simulations have also been observed in the field in many bridges.

Table 3-1: Crack Directionality Results

Δσ [MPa]

Diagonally Into Flange
Diagonally Into Web Plate
Horizontally Into Web Plate
Vertically Into Weld Interface

Material Yielding
Material Fracture
No Crack Growth

	Short Crack Length											
	Web Gap 6.35 mm				Web Gap 12.7 mm				Web Gap 25.4 mm			
	R = 0.0		R = 0.5		R = 0.0		R = 0.5		R = 0.0		R = 0.5	
	Δσ	Cycles	Δσ	Cycles	Δσ	Cycles	Δσ	Cycles	Δσ	Cycles	Δσ	Cycles
Analysis 1	51.5	--	47.4	--	44.5	--	52.3	--	54.4	2.85E+06	54.8	4.40E+06
	67.3	--	67.3	--	67.2	--	67.2	--	68.1	4.58E+06	68.6	--
	80.2	--	78.8	--	82.1	--	82.2	--	77.2	2.32E+06	81.4	--
	106	--	113.2	--	104.5	--	104.7	--	109.2	--	109.5	--
Analysis 2	97.5	--	94.8	--	179.2	--	179.8	9.78E+06				
	128.9	--	129	--	224.1	--	202.4	7.99E+06				
	157.6	--	157.7	4.47E+06	254.1	--	225	5.15E+06				
	200.6	--	198.2	8.91E+06	359	--	357.3	--				

	Medium Crack Length																	
	Web Gap 6.35 mm						Web Gap 12.7 mm						Web Gap 25.4 mm					
	R = 0.0			R = 0.5			R = 0.0			R = 0.5			R = 0.0			R = 0.5		
	$\Delta\sigma$	Cycles		$\Delta\sigma$	Cycles		$\Delta\sigma$	Cycles		$\Delta\sigma$	Cycles		$\Delta\sigma$	Cycles		$\Delta\sigma$	Cycles	
Analysis 1	51.5	--		47.4	--		44.5	--		52.3	--		54.4	--		54.8	9.45E+06	
	67.3	--		67.3	--		67.2	--		67.2	7.42E+06		68.1	--		68.6	9.66E+06	
	80.2	--		78.8	--		82.1	--		82.2	9.85E+06		77.2	8.07E+06		81.4	6.39E+06	
	106	--		113.2	--		104.5	6.61E+06		104.7	6.11E+06		109.2	6.31E+06		109.5	--	
Analysis 2	97.5	--		94.8	--		179.2	7.00E+06		179.8	7.00E+06							
	128.9	--		129	5.17E+06		224.1	5.00E+06		202.4	4.32E+06							
	157.6	--		157.7	5.30E+06		254.1	7.30E+06		225	4.33E+06							
	200.6	7.60E+06		198.2	4.47E+06		359	--		357.3	--							

	Long Crack Length																	
	Web Gap 6.35 mm						Web Gap 12.7 mm						Web Gap 25.4 mm					
	R = 0.0			R = 0.5			R = 0.0			R = 0.5			R = 0.0			R = 0.5		
	$\Delta\sigma$	Cycles		$\Delta\sigma$	Cycles		$\Delta\sigma$	Cycles		$\Delta\sigma$	Cycles		$\Delta\sigma$	Cycles		$\Delta\sigma$	Cycles	
Analysis 1	51.5	--		47.4	--		44.5	--		52.3	--		54.4	9.95E+06		54.8	8.77E+06	
	67.3	--		67.3	--		67.2	--		67.2	5.01E+06		68.1	4.17E+06		68.6	9.97E+06	
	80.2	--		78.8	--		82.1	--		82.2	2.18E+06		77.2	1.48E+06		81.4	8.52E+06	
	106	--		113.2	8.82E+06		104.5	7.40E+06		104.7	9.41E+06		109.2	--		109.5	--	
Analysis 2	97.5	--		94.8	--		179.2	9.71E+06		179.8	3.48E+06							
	128.9	--		129	3.99E+06		224.1	4.34E+06		202.4	1.88E+06							
	157.6	--		157.7	1.74E+06		254.1	5.43E+06		225	1.30E+06							
	200.6	5.91E+06		198.2	6.13E+06		359	--		357.3	--							

Mode III strain energy release rates and information on fatigue loading cycles were obtained from each simulation when the extension of the crack plane occurred. Transformation of the strain energy release rate values into Mode III stress intensity factors was performed for assessment of crack propagation rate results. Crack growth rates were plotted for all models to assess the stability of crack development. Results were analyzed in three different ways to assess crack stability based on the web gap lengths effects, the length of the initial half crack length introduced in the model, and the effect directionality of cracking had on the rate of crack extension. The user defined crack propagation rate equation applied to the numerical simulations has also been inserted into the figures below to provide evaluation for the model to align with anticipated crack propagation behavior.

As seen in Figure 3-10, a web gap of 25.4 mm appears to show less scatter in the da/dN results versus ΔK_{III}. This indicates the tendency of cracks propagating from this web gap length to be controlled by Mode III loading effects and to follow the Paris Law model of crack propagation. High scatter of crack growth rates was noted for web gaps of 6.35 mm and 12.7 mm.

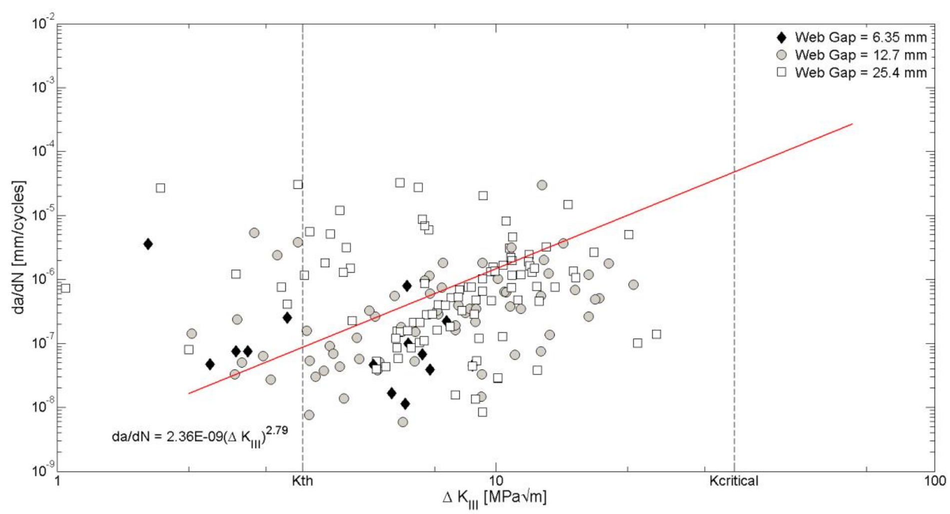

Figure 3-10: Web Gap Length Distinguished Crack Propagation Rate

Horizontal lengths of the initial cracks applied to the models were also seen to affect the stability of crack development. As shown in Figure 3-11 elongation of initial crack lengths aided in stabilizing the rate of crack development to follow a Paris Law crack propagation model. Crack development from an initial half crack length of 6.35mm showed significant scatter when analyzed versus KIII values. Initial half crack lengths of 17.78mm showed the highest correlation to a linear growth rate on a log-log scale.

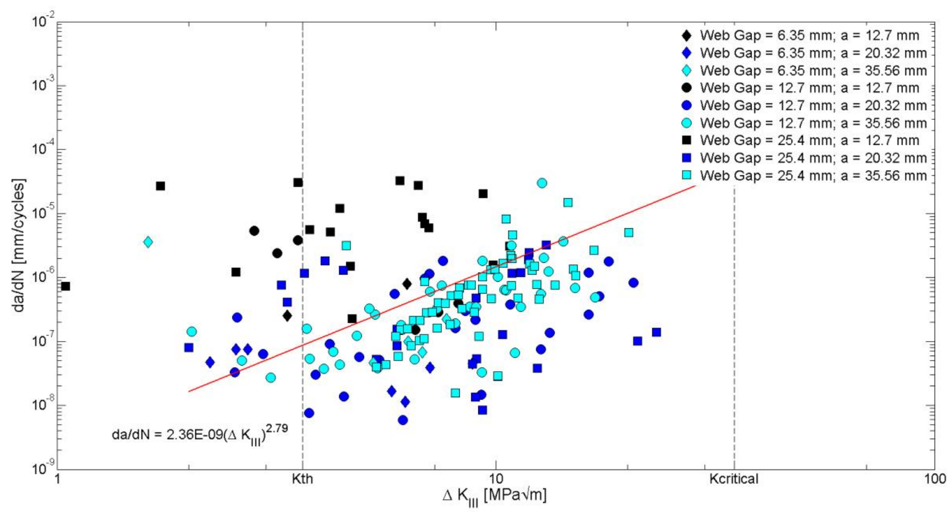

Figure 3-11: Initial Crack Length Distinguished Crack Propagation Rate

Final analysis of crack growth observed the propagation rate due to the directionality of the crack profile Figure 3-12, shown below, illustrates the growth rates of all four crack directionalities seen throughout the simulation models. It was noted that growth occurring horizontally through the web plate material and into the flange interface showed the most stable crack development. It should also be noted that these two crack pathways were seen to occur most often when long initial crack lengths were applied. Horizontal cracking, which shows the most correlation to a Paris Law growth model was also observed to occur only in softer web gap regions of 25.4 millimeters.

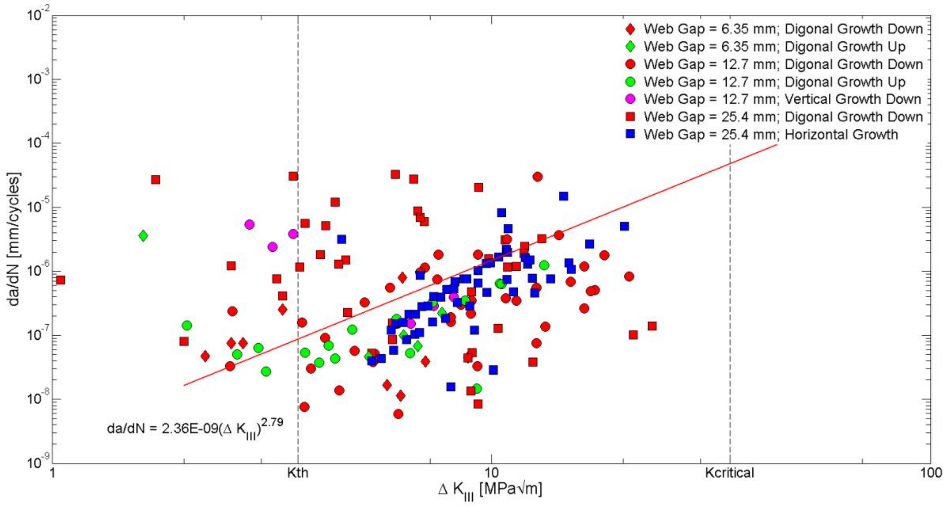

Figure 3-12: Effect of Crack Directionality on Crack Propagation Rate

3.8 Crack Propagation Directionality

The most common orientation of crack elongation developed diagonally through the web material. In some cases, particularly with longer horizontal initial crack lengths, crack directionality was seen to propagate vertically into the flange and web interface. Case study two displacements applied to 12.7 millimeter web gaps for short initial half crack lengths were seen to cause cracking directed vertically down through the web-to-stiffener welding interface. Further analyses showed cracking developing horizontally through the web material away from the web gap region. Horizontal crack propagation was noted to occur only in the largest web gap regions for a 35.56 mm initial crack length.

Results show that the magnitudes of strain energy release rate ratios are the primary variables governing the directionality of crack. Ratios of G_I/G_{IC}, G_{II}/G_{IIC}, and G_{III}/G_{IIIC} were found for each observed crack growth direction to determine the loading mode that had the most contribution to the G_{equiv}/G_{equivC} ratio used in the ABAQUS XFEM analysis. Figure 3-13 shows the location of crack development and the focus region of this study.

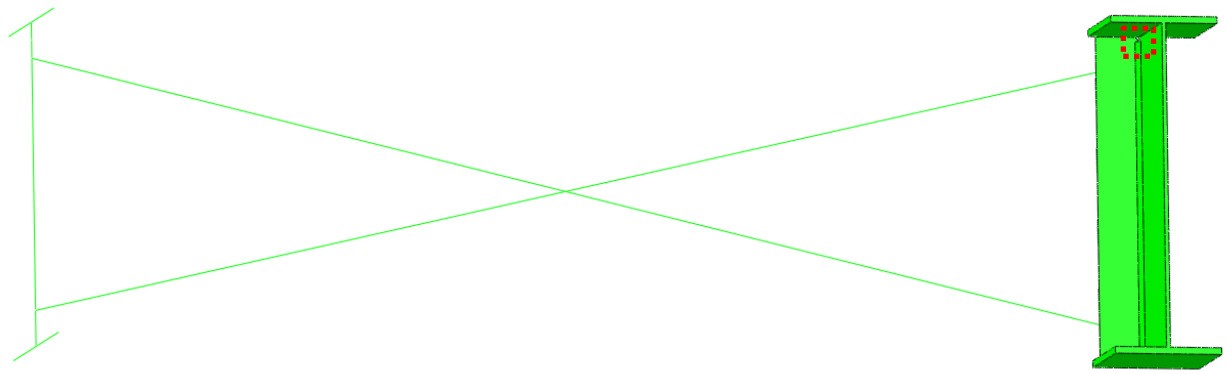

Figure 3-13: Location of Crack Development

Crack propagation that was seen to progress diagonally into the web plate was found to be dominated by Mode I and Mode III effects. Average G_I/G_{IC} and G_{III}/G_{IIIC} for all models cracking in this manner were found to be 0.20 and 0.14 respectively. Average G/G_C values for Mode II were found to be significantly lower at 0.031. Average G_{equiv}/G_{equivC} ratio for this cracking direction was 0.363. Figure 3-14 depicts the G/G_C ratios for all loading models for all models that cracked in a diagonal crack profile into the web material.

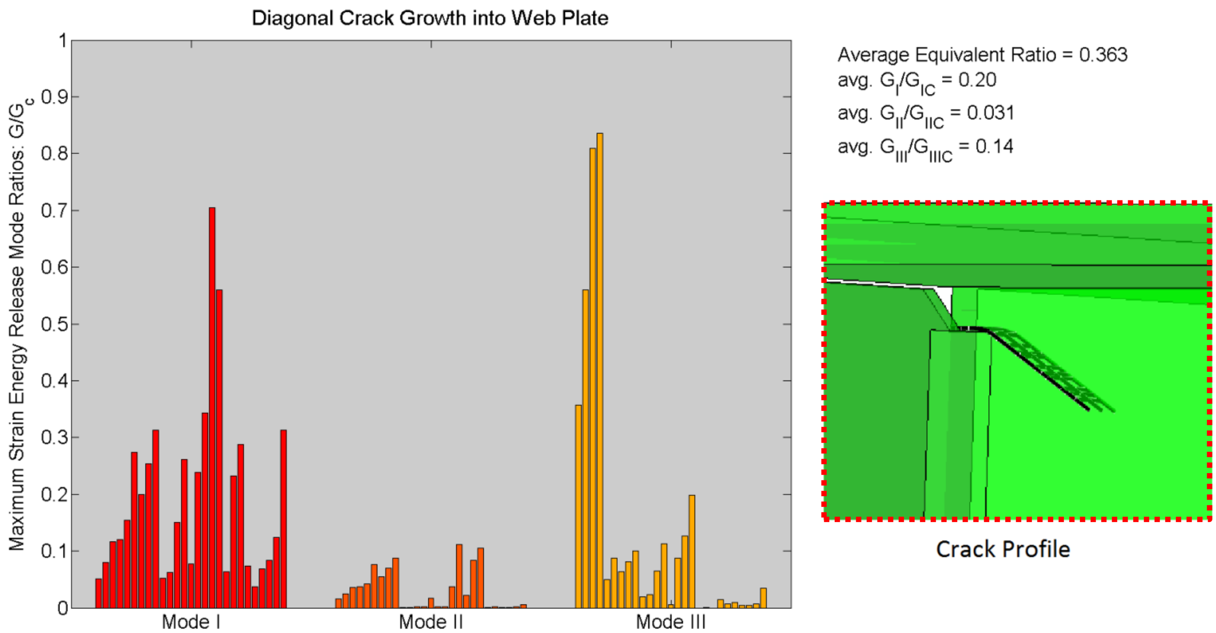

Figure 3-14: Diagonal Downward Crack Growth G/G_C Ratios

A significant shift in G/G_C ratios was noted when values were determined for models that cracked diagonally into the web-to-flange interface. Mode I and Mode III effects were greatly reduced in these models. Mode II effects controlled the growth of the crack with an average G_{II}/G_{IIC} value of 0.17. Equivalent G/G_C values for these models were found to have an average of 0.193. The decrease in the equivalent ratio magnitude was seen to relate to the number of cycles needed to crack the connection material. The lower ratio of G/G_C meant that a larger number of loading cycles had to be applied before cracking occurred. Figure 3-15 shows the ratio magnitudes determined for the thirteen models with this type of cracking.

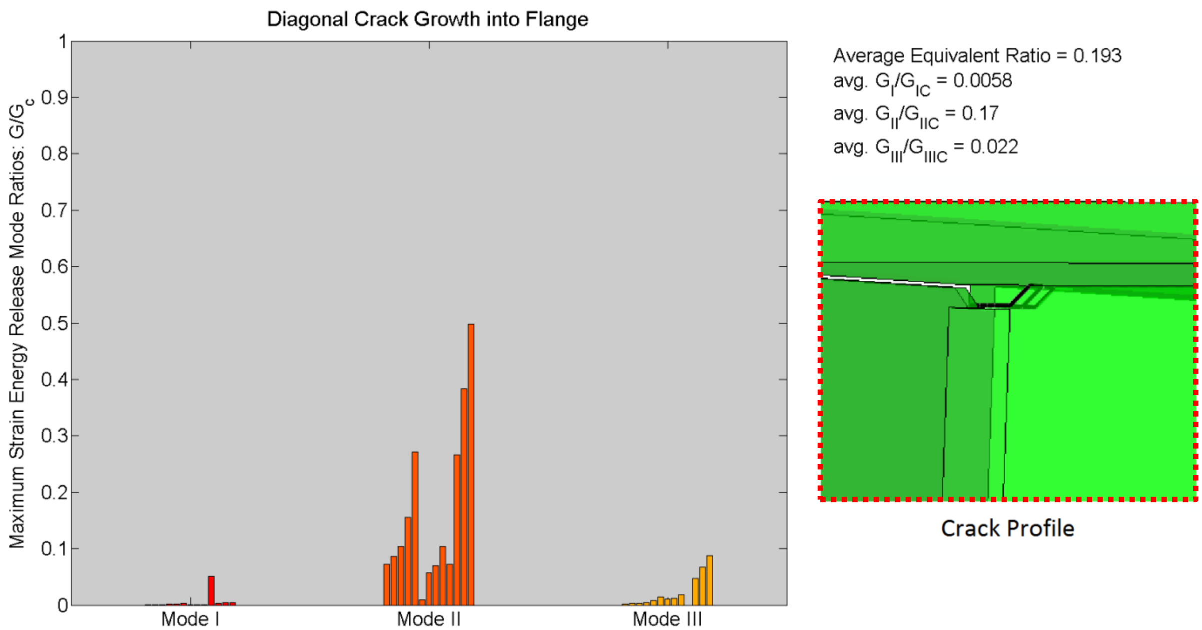

Figure 3-15: Diagonal Upward Crack Growth G/G_C Ratios

Three models were noted to result in vertical crack extension into the weld material connecting the stiffener to the web. Values of strain energy release rates were low for all loading modes however; Mode II effects still dominated the magnitude of the equivalent ratio. Low ratio values also resulted in an increased number of loading cycles needed to crack the material. This result was evident in the simulations of the models cracking vertically. Elongation of the crack was limited to 67.17mm.

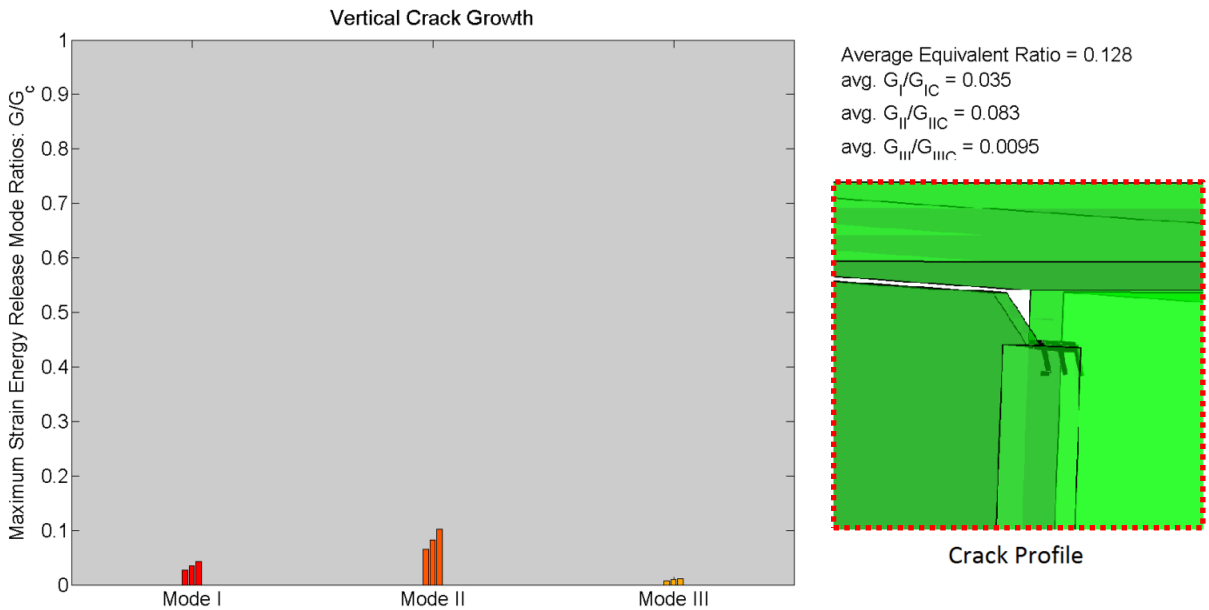

Figure 3-16: Vertical Crack Growth G/G_C Ratios

The final directionality was noted to grow horizontally from the web gap region. This crack pattern was observed only in models with 25.4mm web gap lengths. Mode I and Mode III loading modes dominated the elongation of the crack profile in this crack directionality pattern. Mode II effects were greatly diminished within horizontal cracking. Magnitudes of equivalent G/G_C ratios were on average a value of 0.54. For this crack directionality, Mode III effects controlled the magnitude of the power law relation with an average strain energy release rate ratio of 0.30. Mode II contributions were 120 times lower than Mode III effects with an average value of 0.0024. Figure 3-17 below shows the contribution of the three loading modes to the development of horizontal crack growth.

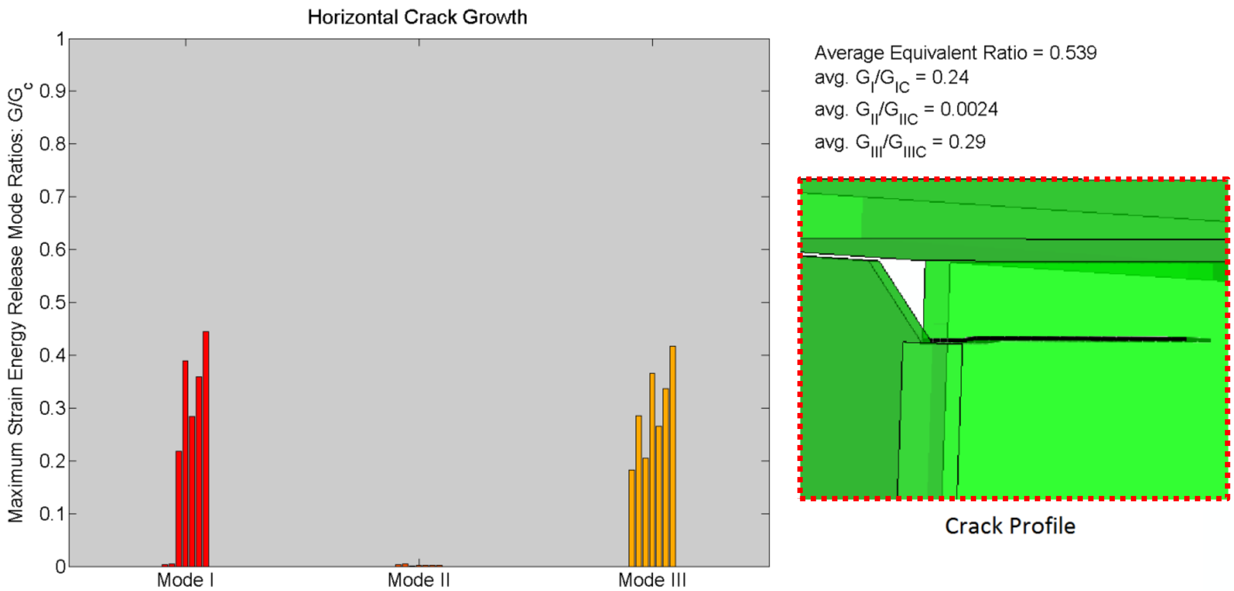

Figure 3-17: Horizontal Crack Growth G/G_C Ratios

Strain energy release rate results were also utilized to determine the cause for crack arrestment seen within the 25.4 millimeter web gap with a 6.35 mm initial half crack length. Results of fatigue simulations on this model yielded unanticipated results; cracking was noted to occur in this model for low applied differential displacement values while application of larger displacements did not result in crack growth. Analysis for these models was made by comparing the G/G_c ratio for each failure mode. Those models that did not result in cracking developed large contributions for Mode II effects in the elements preceding the crack front. Mode I and Mode III strain energy release rate ratios were greatly diminished. It is hypothesized that large Mode II contributions turned the crack propagation direction directly perpendicular of the initial crack plane. This resulted in the crack growing into the stiffener/weld interface. Small magnitudes of G/G_C ratios necessitated high numbers of loading cycles to precipitate cracking. The maximum 10 million loading cycles specified in the analysis were not significant enough to allow for cracking to occur.

3.9 Conclusion

Based on numerical analysis of fatigue crack propagation modeling under the ABAQUS extended finite element analysis method, the following conclusions can be drawn. User defined fatigue resistance classification and crack propagation rate allows for modeling parameters to specify specific testing parameters. Additional inputs of critical and threshold values further allow for users of the numerical software to specify material fatigue characteristics.

Results of Mode I fatigue loading validation studies on A36 steel uniaxial tension geometries showed excellent agreement with experimental results. Simulations were found to match experimental testing of the profile of the crack extension and the rate of crack growth. Given the correct user input information, validation results support the claim that ABAQUS XFEM software can be utilized to model crack propagation due to high cycle fatigue loading events.

Further validation of ABAQUS XFEM capabilities was determined based on studies of crack propagation due to rotational displacement of cylindrical geometries. Failure modes governing crack growth were noted to not be controlled only by Mode III load application. Results of this study illustrated high probability of multi-mode effects directing crack growth. However, results of crack propagation rates illustrated that Paris Law crack propagation theory could be applied to simulate crack growth due to non-Mode I loading effects. Analysis of this validation study noted alignment of crack growth rate results with experimental testing. This conclusion therefore supports that use of Paris Law crack growth theory to model all modes of fatigue loadings.

While simulated results of transverse stiffener results were not able to be corroborated with experimental testing, numerical analysis results provide vital information into fatigue cracking of this connection system. Primary results noted from the conducted analyses are as follows:

- Directionality of crack extension was seen to occur in four primary profiles;
- Termination of crack growth at the web-to-flange interface was found to occur in stiff web gap regions with long initial crack profiles.
- Stable fatigue crack growth of 35.56 mm initial crack lengths was observed in 25.4 mm web gap regions for $\Delta\sigma$ near the CAFL;
- Crack growth occurring diagonally through the web material was the most prevalent crack profile for stiff web gap regions with small initial crack lengths
- Crack growth emanating from small initial crack lengths were seen to result in high scatter of growth rate results for all web gap thicknesses.
- Scatter of crack propagation rate results were noted to be highest for crack extension diagonally through the web material

Results suggest that retrofits of stiffener members exhibiting propagation profiles horizontally through the web plate or into the flange interface are not advisable. Crack arrestment was noted for both of these crack directionalities. Retrofits may adversely affect localized stress concentrations and deformations leading to additional crack growth of the connection detail.

CHAPTER 4

ABAQUS XFEM VALIDATION DISCUSSION

4.1 Validation Studies

4.1.1 Mode I Validation Study

Results of crack propagation due to Mode I fatigue effects were found to provide excellent results when compared to theoretical and experimental observations. Comparative analyses of simulation versus experimental results show that LEFM applied in ABAQUS XFEM software is highly compatible.

Fatigue cracking of both uniaxial tension models was seen to emanate horizontally through the plate material from the machined notch. Crack directionality was consistent with theoretical predictions of crack behavior due to a tensile load application. Stress concentrations were localized around the crack tip, and through the midsection of the plate specimen. Maximum Von Mises stresses within CP_23 were noted to be 1.68 times greater than that of CP_25. In both models maximum Von Mises stress values were located in elements ahead of the crack tip. Figure 4-1 and Figure 4-2 illustrate the directionality of the maximum Von Mises stresses in both models. Stress directionalities have been shown in the figures below at the start of the simulation for the initial crack length, and after the crack profile has propagated through the steel plate material.

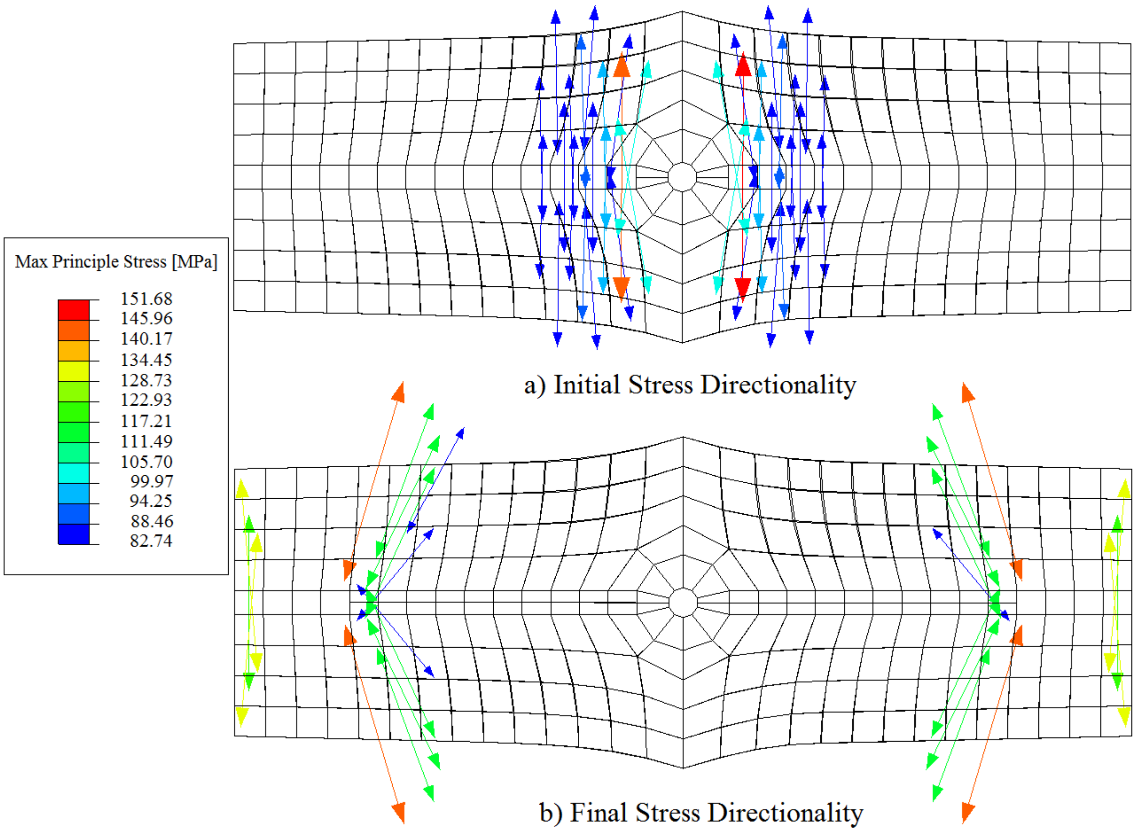

Figure 4-1: CP_23 Maximum Principle Stress Directionality

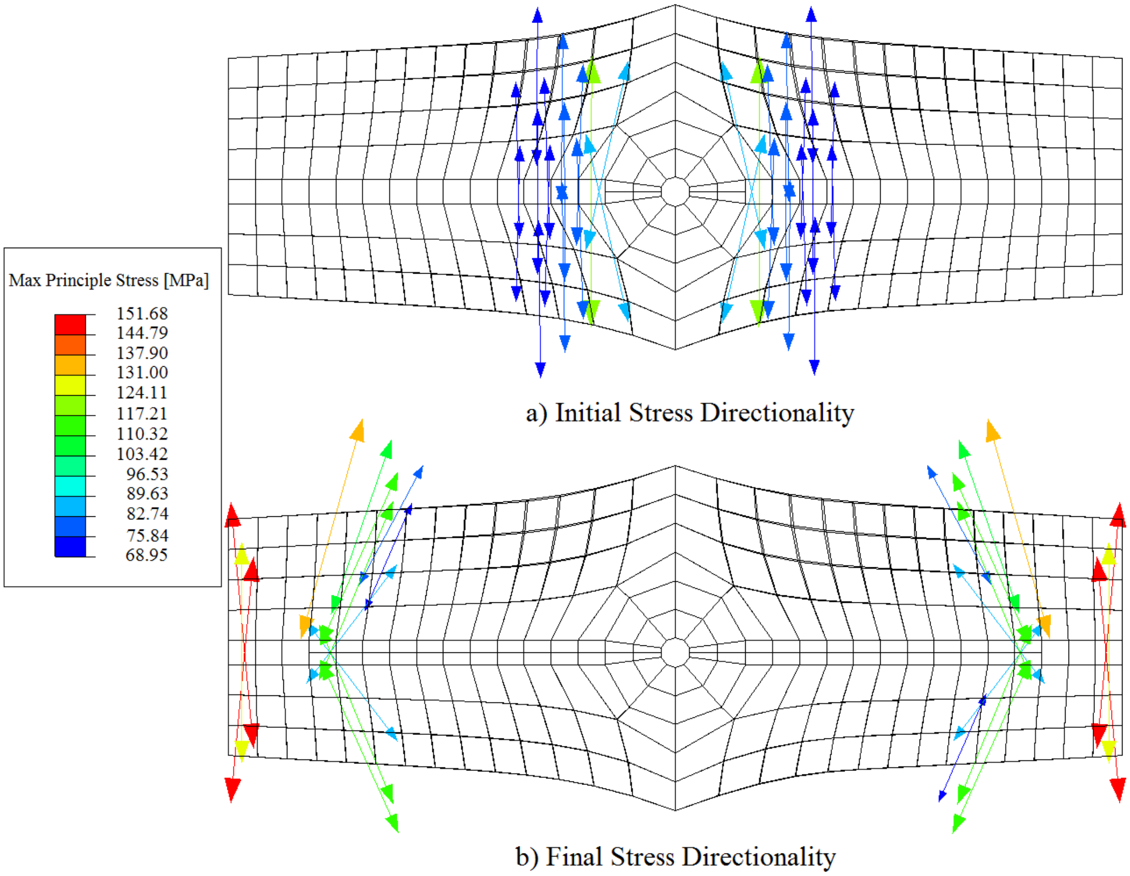

Figure 4-2: CP_25 Maximum Principle Stress Directionality

Slight reorientation of the maximum principle stress was seen to occur at the end of the simulations. However, maximum stress components were consistently oriented perpendicular to both the crack plane and face. Alignment of the stress fields in this manner is indicative of Mode I loaded specimens, and correlates with anticipated theoretical responses. Levels of strain energy release rates for each load cycle in which cracking occurred resulted in maximum Mode II and Mode III G values of $1.85E^{-5}$ and $2.86E^{-5}$ MPa·m respectively. In contrast, maximum G_I values were noted at a magnitude of 2.44 MPa·m for CP_23 model results.

Fatigue resistant classification for both models was determined through a parametric study. Classification was varied throughout each analysis and crack growth results were compared to experimental values. The lowest percent error was shown to occur when a fatigue resistance classification B was applied to model CP_23. Comparatively, a D classification for model CP_25 resulted in the best fit. Differentiation in the classification may be due in part to the quality of the cut that was placed in the experimental geometries that served as the initial crack location. Crack extension results for both models are shown in the following tables.

Table 4-1: Crack Propagation of CP_23 Model

Experimental Results		Model Results	
Half Crack Length [mm]	N [Cycles]	Half Crack Length [mm]	N [Cycles]
5.255	0.00E+00	4.917	0.00E+00
7.399	3.57E+06	7.968	4.07E+06
8.583	4.22E+06	11.019	5.33E+06
9.337	4.70E+06	14.069	6.45E+06
10.505	5.26E+06	17.120	7.24E+06
12.263	5.92E+06	20.170	7.70E+06
12.476	6.00E+06	23.221	7.99E+06
15.334	6.57E+06	26.271	8.17E+06
18.412	7.02E+06	29.322	8.28E+06
26.957	7.52E+06	32.372	8.35E+06
30.307	7.62E+06	35.423	8.39E+06
33.739	7.67E+06		

Table 4-2: Crack Propagation of CP_25 Model

Experimental Results		Model Results	
Half Crack Length [in]	N [Cycles]	Half Crack Length [in]	N [Cycles]
7.463	0.00E+00	7.513	0.00E+00
7.783	7.20E+05	10.378	3.50E+06
8.207	1.69E+06	13.244	7.17E+06
8.463	2.85E+06	16.109	9.71E+06
9.012	4.13E+06	18.974	1.13E+07
9.982	6.00E+06	21.839	1.22E+07
10.856	7.13E+06	24.704	1.29E+07
11.748	8.09E+06	27.569	1.33E+07
12.614	8.76E+06		
13.416	9.41E+06		
14.308	9.92E+06		
15.479	1.06E+07		
16.634	1.11E+07		
17.884	1.15E+07		
19.131	1.19E+07		
20.825	1.24E+07		
22.441	1.27E+07		
24.628	1.31E+07		
27.005	1.34E+07		

Deviation of simulation results from experimental observations was noted in both simulated models. As the crack length of CP_23 grew, results overestimated the fatigue resilience of the material. Beginning stages of crack propagation within CP_25 illustrated underestimation of the fatigue resilience of the steel plate. Maximum percent errors of simulation results were noted to be 9.43% and 36.2% for models CP_23 and CP_25 respectively. Minimum error in each model compared to experimental results was 2.09% and 1.34%. While discrepancies exist between experimental and simulated results, in both cases results show a non-linear increase in crack growth rate. ABAQUS XFEM numerical methods therefore captured characteristic fatigue properties under Mode I loadings.

Further analysis of the model results showed that the simulated fatigue crack propagation matched the rate of crack propagation of experimental data. Maximum percent error of 29.97% was seen within the CP_23 results between the theoretical and simulated results. 26.74% error was also noted as the largest deviation between the theoretical and model within the CP_25 results. Comparative analysis of the simulated to experimental values of ΔK and da/dN are shown in the following three tables. Comparisons were performed by computing the percent error between experimental and model results.

Table 4-3: Threshold Value Comparisons

Threshold Values		CP 23 Results			CP 25 Results		
		Experimental	Model	%Error	Experimental	Model	%Error
$\Delta K_{I,min}$	[MPa√m]	7.91	7.72	2.36	7.03	7.11	1.09
$K_{I,min}$	[MPa√m]	1.87	1.84	1.67	2.31	2.30	0.48
da/dN_{min}	[mm/cycle]	5.99E-7	7.49E-07	25.0	4.47E-7	7.80E-07	75.44

Table 4-4: CP 23 Model ΔKI Comparison

Half Crack Length [mm]	N [cycles]	Theoretical ΔK_I [MPa√m]	Model ΔK_I [MPa√m]	% Error [%]
4.917	0.00E+00	7.72	---	--
7.968	4.07E+06	9.94	12.60	26.74
11.019	5.33E+06	11.89	14.22	19.59
14.069	6.45E+06	13.74	15.55	13.20
17.120	7.24E+06	15.59	17.41	11.63
20.170	7.70E+06	17.54	19.59	11.72
23.221	7.99E+06	19.66	21.83	11.07
26.271	8.17E+06	22.05	24.42	10.71
29.322	8.28E+06	24.89	27.36	9.93
32.372	8.35E+06	28.37	26.50	6.58
35.423	8.39E+06	32.93	30.33	7.91

Table 4-5: CP 25 Model ΔK_I Comparison

Half Crack Length [mm]	N [cycles]	Theoretical ΔK_I [MPa√m]	Model ΔK_I [MPa√m]	% Error [%]
7.513	0.00E+00	7.11	---	--
10.378	3.50E+06	8.48	9.26	9.20
13.244	7.17E+06	9.77	11.68	19.57
16.109	9.71E+06	11.04	12.72	15.22
18.974	1.13E+07	12.36	14.21	14.93
21.839	1.22E+07	13.78	15.82	14.83
24.704	1.29E+07	15.34	17.56	14.47

27.569	1.33E+07	17.12	19.52	13.99

4.1.2 Mode III Validation Study

Validation studies of ABAQUS XFEM compatibility with Mode III fatigue loading effects due to torsional loading corroborated experimental conclusions that Paris Law theory could be applied to Mode III failures. Larger discrepancies between model and experimental results for Mode III failures were reported in contrast to Mode I validation results.

Extension of the initial circumferential crack plane was seen to progress parallel to the cross-section of the model geometry. Development of the crack plane was seen to extend in a circular manner through the material parallel to the initial direction of the crack plane. Maximum principle stress directionalities were seen to align tangent to the crack plane while also emanating out of plane. Orientation of the maximum stress vectors shown in Figure 4-3 were consistent with those induced in material subjected to pure shear effects.

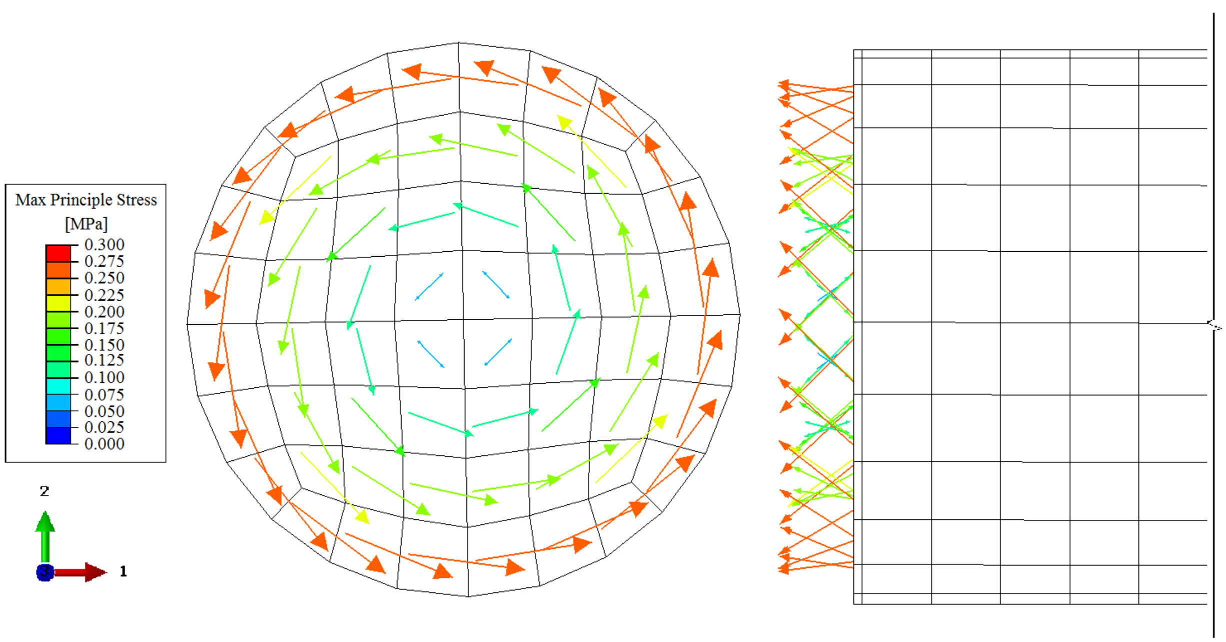

Figure 4-3: Mode III Direction of Maximum Principle Stresses

Mode III loading effects were determined dominate the initial growth of the fatigue crack. Once failure of the material progressed to the central element of the geometry, strain energy release values for all loading modes were of consistent magnitude. Therefore it is anticipated that this fatigue loading does not adhere to a singular failure mode analysis throughout the entirety of the analysis. Results of Mode III ΔK values between experimental, simulated, and theoretical results further illustrate the multi-mode loading effects of the model. Percent errors between theoretical values and simulated results are shown below in Table 4-6. For the two models displaced with the largest rotation, this error coincided with the point at which Mode I and Mode II strain energy release rate values increase substantially. Smaller rotational displacements were noted to decrease magnitudes of Mode I and II strain energy release rates, and were closer to modeling a singular failure mode through Mode III effects.

Table 4-6: Mode III Crack Propagation Rate Results

Rotation = 0.02 [radians]

Half Crack Length [mm]	N [cycles]	dc/dN [mm/cycle]	Theoretical ΔK_{III} [MPa√m]	Model ΔK_{III} [MPa√m]	% Error [%]
3.2243	3.36E+05	3.86E-06	8.18	8.01	2.08
4.5226	3.89E+05	2.46E-05	13.28	10.62	20.03
4.5295	3.55E+05	3.67E-06	13.32	10.94	17.87
4.6144	2.36E+05	6.52E-06	13.78	13.07	5.15
6.3537	6.12E+05	8.22E-06	30.56	24.11	21.11
6.3641	2.36E+05	2.42E-05	30.73	27.37	10.93
7.6906	6.12E+05	2.35E-05	66.89	26.31	60.67

Rotation = 0.0325 [radians]

Half Crack Length [mm]	N [cycles]	dc/dN [mm/cycle]	Theoretical ΔK_{III} [MPa$\sqrt{m}$]	Model ΔK_{III} [MPa$\sqrt{m}$]	% Error [%]
3.2243	1.49E+05	8.69E-06	8.18	10.58	29.34
4.5226	1.72E+05	5.70E-05	13.28	14.07	5.95
4.5295	1.60E+05	8.12E-06	13.32	14.67	10.14
4.6144	2.18E+05	7.06E-06	13.78	27.64	100.58
4.6144	5.07E+05	3.03E-06	13.78	21.81	58.27
6.1525	5.46E+05	3.95E-05	27.57	18.57	32.64
6.3537	2.36E+05	2.87E-05	30.56	32.58	6.61
7.6906	2.36E+05	9.51E-05	66.89	29.60	55.75

Rotation = 0.0365 [radians]

Half Crack Length [mm]	N [cycles]	dc/dN [mm/cycle]	Theoretical ΔK_{III} [MPa$\sqrt{m}$]	Model ΔK_{III} [MPa$\sqrt{m}$]	% Error [%]
3.2243	1.49E+05	8.69E-06	8.18	10.58	29.34
4.5226	1.73E+05	5.48E-05	13.28	14.06	5.87
4.5295	1.60E+05	8.12E-06	13.32	14.68	10.21
4.6144	2.19E+05	7.04E-06	13.78	27.62	100.44
4.6144	2.35E+05	6.54E-06	13.78	13.07	5.15
6.3537	2.35E+05	2.94E-05	30.56	32.57	6.58
6.3641	2.35E+05	2.45E-05	30.73	27.38	10.90
7.6906	2.35E+05	9.57E-05	66.89	29.61	55.73

CHAPTER 5

CONCLUSION & FUTURE WORK

Current transportation infrastructure systems across the United States are in dire need of rehabilitation and restoration efforts. Constant application of loadings is one facet that has contributed to degradation of bridge super structures across the country. The effects of out of plane distortion at transverse connection systems has resulted in fatigue crack development within bridge girder members. High percentages of operation bridges exhibit signs of fatigue crack growth. Limited experimental research has been conducted on the fatigue crack characteristics of these fatigue prone details. Consequently, limited rehabilitation measures are used to attenuate crack development of the girder material.

Numerical analysis through finite element modeling of transverse connection geometries was proposed as a potential method to study cracking characteristics of the connection detail. ABAQUS XFEM methodology was offered as a useful tool to track crack growth due to high cycle fatigue loadings of the connection. User defined fatigue resistance classification and crack propagation rates were hypothesized to allow for development of model simulations that mimicked physical test scenarios. Validation of numerical software was conducted based on the primary failure modes of the transverse stiffener connection: Mode I and Mode III.

Analysis of modeling capabilities due to Mode I fatigue loading was conducted on high cycle uniaxial fatigue loading of steel plates. An experimentally defined crack propagation rate was utilized to define the fatigue behavior of the material. Further classification was defined through AASHTO S-N curve crack resistance parameters. Correlation of experimental and simulated results was noted for both crack directionality and crack growth rates.

Mode III software validation was conducted based on torsional fatigue loadings on cylindrical steel specimen. Experimental results hypothesized that the rate of propagation for Mode III loadings could be expressed in terms of the alternating stress intensity factor; ΔK. This result correlates with use of the Paris Law growth rate specification for Mode I analyses. Results of the simulations determined that Mode III loading effects were not the sole contributing factor to crack development. Alignment of simulated crack rate development results; however, was noted when compared against experimental test results. This result determined that multi-mode fatigue loading effects could be idealized based off of the Mode I Paris Law equation.

Justification for applying the Paris Law crack propagation rate theory has extreme implications to the study of fatigue crack development. From this finding, it was determined that ABAQUS XFEM is capable of modeling fatigue in material geometries not controlled by Mode I loading alone. Therefore, modeling of crack propagation in transverse stiffener connections was believed to be possible. Beyond the scope of this research project, ability to use this numerical software for fatigue analysis could be applied to all manner of fatigue problems.

Simulation of transverse stiffener connections was performed to analyze the following variable effects on fatigue crack development. Studies were run to observe the effects that web gap stiffness had on fatigue resistance of the connection. Various displacements were applied to the models to observe the effects that localized stress concentrations would have on crack development. Analyses were run on stress range levels near the constant amplitude fatigue limit for C rated fatigue resistant details. Worst case scenario simulations were also conducted to observe the effects that high displacements would have on stiffer web gap regions. Finally, initial crack lengths within the web gap regions were varied to observe the effects that initial crack length had on fatigue of the bridge superstructure material.

Under case study one stress ranges, no cracking was observed in stiffer web gap regions for low stress ranges for all initial crack lengths. A higher probability of cracking was seen to occur in web gap lengths of 25.4 millimeters. Cracking was noted in 25.4 mm web gap regions for stress ratios at and below the 69 MPa (10 ksi) CAFL for C rated fatigue details. Cracking at stress levels near the CAFL may be due to the connection detail softening resulting in heightened levels of distortion at the web gap which promote crack growth.

Elongated crack lengths were seen to alter crack profile directionalities in stiff web gap regions. This resulted in less sever cracking occurring. Analysis of case study two loadings showed crack directionality to progress vertically into the flange interface within the stiffer web gap models with long initial crack lengths. Cracking in this manner was seen to be governed by Mode II loading effects. The ability for the crack profile to progress into a Mode II dominate failure may be ideal in arresting crack development for stiffer connections. From the simulated results it is suggested that within a stiff web gap region, slight elongation of the initial crack may result in heightened levels of Mode II loading effects that result in crack directionality shifts that arrest crack development. Due to crack redirection into the flange profile, retrofitting transverse connection details is not necessary as the crack arrests once the profile enters a region of increased material thickness.

Cracks in 25.4 mm web gap regions with initial crack lengths of 35.56 mm propagated horizontally into the web plate material for all applied stress ranges. Propagations of crack profiles in this manner were found to be dominated by Mode I and Mode III loading effects. High final crack lengths were observed in all of these simulations. However, this crack development also corresponded to stable crack growth. From the results of these simulations it is hypothesized that manually directing crack profiles horizontally through the web plate will encourage stable crack growth in softer web gap regions. If crack enlargement is not interrupted by rehabilitation efforts, cracks are expected to arrest once the profile enters a low stress region of the web plate.

While simulated results suggest lengthening crack profiles horizontally will arrest crack growth; significant research must be conducted to validate the findings of this research project. Minimal experimental testing has been conducted on out-of-plane distortion cracking. The majority of experimental research focuses on crack initiation of transverse connections. Due to limitations in available research and funding to support experimental testing, models developed to assess fatigue cracking of transverse stiffeners were not analyzed against physical results and should not be solely relied upon.

The researcher recognizes that there is significant future work that must be conducted to truly analyze and understand fatigue of transverse stiffener systems. Primary research to be performed encompasses experimental testing of crack development within the detail. Specifically, data must be obtained on the progression of crack growth in the material. Information on the crack length per load cycle is imperative to understand the character of the fatigue crack. Instrumentation of experimental tests must also be performed to better understand the stress intensity factors developed due to the crack presence. This information in conjuncture with crack elongation data would allow for the determination of a theoretical rate of crack propagation for transverse stiffener details. Development of experimental crack growth rate results would also ensure if Paris Law methodology should be applied to this failure analysis. While Paris Law has been noted to be valid for Mode III effects, multi-mode loadings may alter application of this modeling approach.

Additional work is proposed to further assess the effect that crack redirection has on fatigue resistance. The conducted research focused on only one form of crack alteration; horizontal extension. It is thought that insertion of differing crack profiles may also arrest crack growth for a multitude of web gap lengths. Crack propagation may slow significantly if a vertical crack profile was inserted at the tip of the initial fatigue crack. Introduction of this crack profile is hypothesized to increase the effect that in-plane horizontal stresses have on crack elongation. For stiffer web gap regions crack directionality is hypothesized this will result in quick crack arrestment. Additionally, cracking of softer web gap regions may arrest sooner but still maintain stable crack growth.

WORKS CITED

AISI Example 2: Two-Span Continuous Composite I Girder. American Iron and Steel Institute, 1997.

Altay, A. K., D. S. Arabbo, E. B. Corwin, and R. J. Dexter. *Effects of Increasing Truck Weight on Steel and Prestressed Bridges.* Report MN/RC-2003-16, 2003.

ASCE. "2013 Report Card of America's Infrastructure." 2013.

Barbero, Ever J. "Finite Element Analysis of Composite Materials with Abaqus." In *Finite Element Analysis of Composite Materials with Abaqus*, by Ever J. Barbero, 362. CRC Press, 2013.

Bowman, M.D., G. Fu, Y.E. Zhou, R.J. Connor, and A.A Godbole. *NCHRP Report 721: Fatigue Evaluation of Steel Bridges.* Washington, D.C.: Transportation Research Board, 2012.

Castiglioni, C.A., J.W. Fisher, and B.T. Yen. "Evaluation of Fatigue Cracking at Cross Diaphragms of a Multigirder Steel Bridge." *Journal of Construction Steel Research,* 1988: 95-110.

CDOT. *Traffic Data Explorer.* 2014. http://dtdapps.coloradodot.info/Otis/.

Chen, Wai-Fah, and Lian Duan (Eds.). *Bridge Engineering Handbook.* Boca Raton, FL: Taylor & Francis Group, 2014.

Connor, R.J., and J.W. Fisher. "Identifying Effective and Ineffective Retrofits for Distortion Fatigue Cracking in Steel Bridges Using Field Instrumentation." *Journal of Bridge Engineergin*, 2006: 745-752.

Dr. Abadi, Ali. *Chapter Four: Mechanical Properties of Materials.* Lecture Notes, University of Technology, n.d.

Federal Register Rules and Regulations. Federal Highway Administration, 2004.

Fisher, J. W., H. Hausmann, M.D. Sullivan, and A.W. Pense. *NCHRP Report 206: Detection and Repair of Fatigue Damage in Welded Highway Bridges.* Washingtion, D.C.: Transportation Research Board of the National Academies, 1979.

Fisher, John W. "Fatigue Cracking in Bridges from Out-of-Plane Displacements." *Canadian Journal of Civil Engineering* (Lehigh University), 1978: 542-556.

Fisher, John W. *NCHRP Report 336: Distortion-induced Fatigue Cracking in Steel Bridges.* Washington, D.C.: Transportation Research Board, 1990.

Fisher, John W., and Peter B. Keating. "Distortion-Induced Faigue Cracking of Bridge Details with Web Gaps." *Journal of Construction Steel Research*, 1989: 215-228.

Fraser, Robert E.K., Gilbert Y. Grondin, and Geoffery L. Kulak. *Behavior of Distortion-Induced Fatigue Cracks in Bridge Girders.* Structural Engineering Report No. 235, Edmonton, Alberta, Canada: University of Alberta, 2000.

Fu, C.C., Yunfeng Zhang, F.G. Yuan, and Ed Zhou. "Integrated Structural Health Monitoring." *University of Maryland Department of Civil and Environmental Engineering.* n.d.

Ghahremani, Kasra , Ayan Sadhu, Scott Dr. Walbridge, and Sriram Dr. Narasimhan. "Fatigue Testing and Structural Health Monitoring of Retrofitted Steel." 2012.

Gilmour, RADM Thomas H., and et.al. *Predicting Stable Fatigue Crack Propagation in Stiffened Panels.* Ship Structure Committee SSC-435 , 2004.

Grubb, Michael E., and Robert E. Schmidt. "Example 1: Three-Span Continuous Straight Composite I Girder Load and Resistance Factor Design." Technical Report, 2004.

Hassel, H. L., C.R. Bennett, A.B. Matamoros, and S.T. Rolfe. "Parametric Analysis of Cross-frame Layout on Distortion-Induced Fatigue in Skewed Steel." *Journal of Bridge Engineering*, 2013: 601-611.

Hellier, A.K., K. Zarrabi, and A.A. Merati. "On the Mode II Fatigue Threshold for Mild Steel." *International Journal of Fracture*, 2011: 267-272.

Hu, Yuying, Carol K. Shield, and R. J. Dexter. *Use of Adhesives to Retrofit Out-of-Plane Distortion Induced Fatigue Cracks.* MN/RC-2006-04, 2006.

Jie-Oing, Wu. "Fracture Curve of a Thin-Walled Tube in Torsion Test." Huston, Texas, 1989.

Klingerman, David J., and John W. Fisher. "Threshold Crack Growth in A36 Steel." Fritz Laboratory Reports, Lehigh University, 1973.

Lukáš, P., and L. Kunz. "Role of Persistent Slip Bands in Fatigue." *Philosophical Magazine*, 2004: 317-330.

Mahmoud, Dr. Hussam. *Fatigue Due to Secondary Stresses.* PowerPoint Presentation. Colorado State University, Fort Collins, CO. 2013.

Mahmoud, Hussam N., S. Meagher, and B.T. Yen. *Results of Field Measurements of the Pearl Harbor Memorial Bridge on I-467 over the Schuylkill River.* Interim Report, ATLSS Interim Report #06-07, Lehigh University, 2006.

Paris, P.C., M.P. Gomez, and W.P. Anderson. "A Rational Analytic Theory of Fatigue." *The Trend in Engineering*, 1961: 14.

Reeder, James R. *3D Mixed-Mode Delimination Fracture Criteria - An Experimentalist's Perspective.* Hampton, VA: National Aeronautics and, 1992.

Ritchie, R.O., and et.al. "Fatigue Crack Propagation in Low Alloy Steel." *Americal Society of Metals and he Metallurgical Society of AIME*, 1982: 101-109.

Roylance, David. *Fatigue.* Cambridge, MA: Massachusetts Institute of Technology, 2001.

Ryan, Thomas, W., J. Eric Mann, Zachary M. Chill, and Bryan T. Ott. *Bridge Inspector's Reference Manual.* Technical Report, Arlington, VA: Federal Highway Administration, 2012.

Simulia, Dassault Systèmes. ABAQUS FEA Version 6.12. Providence, RI. 2012.

Vethe, Stine. *Numerical Simulation of Fatigue Crack Growth.* Norwegian University of Science and Technology, 2012.

Yue, Jireh J. "Energy Concepts for Fracture." *Laboratory for Scientific Visual Analysis.* July 29, 2009. http://www.sv.vt.edu/classes/MSE2094_NoteBook/97ClassProj/anal/yue/energy.html (accessed August 26, 2013).